# A Highly Conserved *Shh* Enhancer Coordinates Hypothalamic and Craniofacial Development

Zoe Crane-Smith[1†], Jeffrey Schoenebeck[2], Katy A. Graham[1], Paul S. Devenney[1], Lorraine Rose[1], Mark Ditzell[3], Eve Anderson[1†], Joseph I. Thomson[1], Natasha Klenin[4], Deborah M. Kurrasch[4], Laura A. Lettice[1] and Robert E. Hill[1]*

[1] Medical Research Council Human Genetics Unit, Institute of Genetics and Molecular Medicine, University of Edinburgh, Edinburgh, United Kingdom, [2] The Roslin Institute and Royal (Dick) School for Veterinary Studies, University of Edinburgh, Edinburgh, United Kingdom, [3] Cancer Research UK Edinburgh Centre, Institute of Genetics and Molecular Medicine, University of Edinburgh, Edinburgh, United Kingdom, [4] Department of Medical Genetics, Alberta Children's Hospital Research Institute and Hotchkiss Brain Institute, University of Calgary, Calgary, AB, Canada

Enhancers that are conserved deep in evolutionary time regulate characteristics held in common across taxonomic classes. Here, deletion of the highly conserved *Shh* enhancer SBE2 (*Shh* brain enhancer 2) in mouse markedly reduced *Shh* expression within the embryonic brain specifically in the rostral diencephalon; however, no abnormal anatomical phenotype was observed. Secondary enhancer activity was subsequently identified which likely mediates low levels of expression. In contrast, when crossing the SBE2 deletion with the *Shh* null allele, brain and craniofacial development were disrupted; thus, linking SBE2 regulated *Shh* expression to multiple defects and further enabling the study of the effects of differing levels of *Shh* on embryogenesis. Development of the hypothalamus, derived from the rostral diencephalon, was disrupted along both the anterior-posterior (AP) and the dorsal-ventral (DV) axes. Expression of DV patterning genes and subsequent neuronal population induction were particularly sensitive to *Shh* expression levels, demonstrating a novel morphogenic context for *Shh*. The role of SBE2, which is highlighted by DV gene expression, is to step-up expression of *Shh* above the minimal activity of the second enhancer, ensuring the necessary levels of *Shh* in a regional-specific manner. We also show that low *Shh* levels in the diencephalon disrupted neighbouring craniofacial development, including mediolateral patterning of the bones along the cranial floor and viscerocranium. Thus, SBE2 contributes to hypothalamic morphogenesis and ensures there is coordination with the formation of the adjacent midline cranial bones that subsequently protect the neural tissue.

**Keywords:** *Shh,* enhancer, hypothalamic development, craniofacial formation, embryonic development

# INTRODUCTION

Long-distance enhancers that are conserved across multiple classes of vertebrates are implicated in regulating early embryonic development (Nord et al., 2013). The *Shh* regulatory domain, which extends 1 Mb upstream of the gene contains a number of sequence elements identified by high sequence conservation. These elements appear to be largely responsible for the typical pattern of *Shh* expression observed at initial stages of organogenesis (Jeong et al., 2008; Anderson et al., 2014). The deep conservation and early stages of expression mediated by these *Shh* enhancers suggest a fundamental role in generating ancient, shared vertebrate characteristics. Studies to date show a modular composition of the *Shh* regulatory domain and thus, for at least some of the *cis*-regulators, there is a simple relationship of a single enhancer to a distinct spatial domain of expression (Jeong et al., 2006; Lettice et al., 2014); although, in other instances, secondary enhancers provide compensatory low levels of expression (Tsukiji et al., 2014; Letelier et al., 2018).

SHH is a signalling factor with a fundamental role in brain and craniofacial development. A number of enhancers have been identified within the *Shh* regulatory domain that are responsible for regulating expression in the midbrain and forebrain. Transgenic analysis indicates that the SBE2 enhancer (Jeong et al., 2006, 2008; Zhao et al., 2012) regulates *Shh* expression in the early developing forebrain, from the zona limitans intrathalmica (ZLI) to the medial ganglionic eminence (MGE), specifically within the rostral diencephalon (Jeong et al., 2006; Zhao et al., 2012). Of particular interest is a clinically relevant inactivating mutation in the SBE2 enhancer associated with features of semilobar holoprosencephaly (Jeong et al., 2008). Holoprosencephaly (HPE) is a developmental disorder of both the forebrain and midline facial structures that include microcephaly, midfacial hypoplasia, cleft lip and palate and moderate fusion of the hypothalamus and occasionally includes the condition of diabetes insipidus (Marcorelles and Laquerriere, 2010). More commonly, HPE is associated with heterozygous mutations that inactivate the *Shh* gene (Chiang et al., 1996; Ming and Muenke, 2002). These data suggest that disruption of SBE2 driven expression in the early developing forebrain may contribute to this disorder (Jeong et al., 2008).

Here, we deleted the SBE2 enhancer to discern its overall contribution to the *Shh* expression pattern and to establish its requirement for mediating the embryonic phenotype. *Shh* expression is continuous throughout the central nervous system, relying on a number of *cis*-regulators to generate the overall pattern (Anderson et al., 2014). The deletion of SBE2 interrupted this spatial pattern by specifically downregulating expression in the ventral portion of the rostral diencephalon; however, this reduction of SBE2 driven *Shh* expression produced no overt phenotype. We confirmed the presence of a second enhancer (Sagai et al., 2019) responsible for residual levels of *Shh* expression that compensated for the loss of SBE2 in the rostral diencephalon. Further reduction in expression levels of *Shh* was attained by crossing the SBE2 deletion mice to the line carrying the *Shh* null allele. The development of the hypothalamus and of the surrounding tissue was disrupted in the compound

mutants, linking diencephalic spatiotemporal expression to multiple defects and enabling analysis of development at different expression levels. We showed, firstly, that low levels of *Shh* are sufficient for patterning in the hypothalamus along the AP axis to occur. Further reductions in the levels of *Shh*, however, led to misplaced spatial assignment of the hypophyseal lobes due to disruption of the AP boundary. Secondly, gene expression along the DV axis was, in contrast, concentration sensitive and consistent with SHH functioning as a morphogen along this developmental axis, with tissue patterning and eventual neuronal fate reliant upon varying concentrations of *Shh* signalling. Thirdly, we found that loss of SBE2 activity disrupts craniofacial development affecting mediolateral patterning of the bones along the cranial floor and palatal shelf, revealing that SBE2 activity in the brain regulates cranial and facial morphogenesis, providing further evidence of the ventral patterning role played by *Shh* (Dworkin et al., 2016; Corman et al., 2018). Hence, a single regulatory component coordinates the combined function of directing brain development with the concomitant role of ensuring physical neuroprotection.

# MATERIALS AND METHODS

## Embryo Production and Transgenic Targeting

All animal experiments were reviewed and approved by the University of Edinburgh Animal Welfare and Ethics Committee and were conducted with appropriate licensing under Animals (Scientific Procedures) Act 1986.

The $Shh^{null}$, $Shh^{\Delta SBE2}$ (described below) and SBLac526 lines were maintained on a C57BL/6J background and crossed to this strain for at least 5 generations prior to experimental collection. Embryos were harvested at various embryonic stages between E9.5 and E17.5. For all experiments described triplicate datasets were used, unless otherwise stated. Heterozygous loss of *Shh*, $Shh^{null/+}$, is known to cause no phenotypic effects (Chiang et al., 1996). Nevertheless differences between wild-type, $Shh^{\Delta SBE2/+}$ and $Shh^{null/+}$ embryos were assessed. As expected, no differences were detected between the three previously mentioned genotypes. Unless otherwise stated, control embryos were $Shh^{+/+}$ wild-types.

The expression driven by a potential enhancer region of interest was analysed in G0 transgenic embryos using a *lacZ* construct which carried sequence of the region in question, a β-globin minimal promoter and *lacZ* as has been previously described (Yee and Rigby, 1993). The DNA fragment of interest was generated using PCR with the primers GATCAT**GTCGAC**GCTCCAGGTACTGCTGTTCAG and GAT CAT**GCTGAC**ATGTGGATGGCAAGCATTGGC- the *Sal*I restriction site used in the cloning is highlighted in bold.

## ATAC-Seq and FAC Sorting

Entire heads of GFP positive eGFP/Cre-*Shh* (Harfe et al., 2004) embryos were dissected and single cell suspensions were made by incubating the dissected tissue in 1:5 dilution of trypsin:versene

at 37°C for 15 min. GFP positive cells were sorted using a fluorescence activated cell sorter and ATAC-seq libraries were made from the positive cell population pooled across littermates as previously described (Buenrostro et al., 2015). Subsequently libraries were subject to size selection to exclude DNA fragments larger than 1 kb using SPRIselect magnetic beads (Beckman Coulter). Samples were sequenced on a Illumina HiSeq 4000 platform to obtain 50 bp paired-end reads. Resulting reads were trimmed using cutadapt paired-end trimming, and subsequently aligned to the mm9 mouse genome using bowtie2 paired-end alignment. Unmapped reads and those mapping to the mitochondrial genome were then removed and duplicate reads were filtered out using Picard MarkDuplicates. Reads were shifted by +4 bp for those mapping to the positive strand and −5 bp for those mapping to the negative strand. Broad peaks were then called, to identify open chromatin regions, using MACS2 callpeak, using –g mm, -f BEDPE, -B –broads and cutoff 0.01 options. The ATAC-seq data have been deposited at the NCBI Gene Expression Omnibus (GEO) database (GEO accession number: GSE158074).

## SBE2 Deletion Line Production by CRISPR

CRISPR guide oligo pairs were designed flanking the SBE2 enhancer region described by Zhao et al. (2012). The pairs were annealed and cloned into the pX330 vector.

Guide sequences used were: Upstream of SBE2, 5′ AAACACA TTAAAGCCCTCCAGCG 3′ and 5′ CACCGACGCTGGA GGGCTTTAATGT 3′; Downstream of SBE2, 5′ AAACACGAG CAAGCCAACCGGAGG 3′ and 5′ CACCGCTCCGGTTGGCT TGCTCGT 3′. pX330-U6-Chimeric_BB-CBh-hSpCas9 was a gift from Feng Zhang (Addgene plasmid # 42230[1]; RRID:Addgene_42230) (Cong et al., 2013).

Transgenic mice were made by pronuclear injection of plasmid DNA into C57BL/6J × CBA F2 embryos. G0 pups were genotyped by PCR and sequencing. Pups carrying the correct deletions were then used to establish the line by mating to C57BL/6J mice.

## OPT Analysis

OPT imaging was performed (Sharpe, 2003). Briefly, PFA-fixed embryos were embedded in 1% low-melting-point agarose and dehydrated by immersion in methanol for 24 h. The samples were cleared for 24 h in BABB (one part benzyl alcohol/two parts benzyl benzoate). Samples were then scanned using a Bioptonics 3001 scanner[2], images taken every 0.9° (of a 360° rotation) and were reconstructed using Bioptonics proprietary software with the outputs then being viewed with Dataviewer (Bioptonics) and Bioptonics Viewer.

## Morphometric Analysis

MicroCTs of fifteen E17.5 embryos (7 controls, 8 mutants) collected from three litters were scanned post mortem using a Bruker Skyscanner 1076. Individual skull scans

[1]http://n2t.net/addgene:42230

[2]www.biooptonics.com

were downsampled 2:1 using Bruker NRecon. Reconstructed images were converted to DICOM format using Bruker DicomCT. Twenty-eight landmarks were placed on each isosurface using Stratovan CheckPoint (v19.03.04.1102 Win64). In two mutants, dysmorphology of the vomer prevented placement of corresponding landmarks and as such, the landmarks were indicated as "missing." Raw coordinates data saved in Morphologika format were processed in R (v4.0.2) using Geomorph (v3.3.2), Rvcg (v0.19.2), Morpho (v2.8), and Hotelling (v1.0-5) packages. Missing landmarks were estimated using a multivariate regression method implemented in Geomorph. Following, a Generalised Procrustes analysis (GPA) was translated, rotated and rescaled raw landmark coordinate data to minimise the sum of squared distances between specimens. The amount of rescaling required in the GPA is captured by the centroid size, a variable which is used subsequently as a proxy for specimen size. A single outlier (control, Litter 3) was removed as its Procrustes distance was >1 standard deviation from the mean. Following removal of the outlier, the GPA was rerun to produce Procrustes shape residuals. Model effects of shape, genotype, size and litter were tested using the non-parametric method of multivariate ANOVA implemented in Geomorph. Significant model effects included size, genotype and litter nested in genotype; the best model was described by coordinates ∼log(centroid size)+ genotype/litter.

In order to visualise shape differences, a randomly chosen ply surface file was warped using thin plate splines using the mean coordinate values of all fourteen specimens. The resulting mesh represented the dataset reference which was subsequently warped to using principal component minimum and maximum shape variables.

## Tissue Processing

Embryos were dissected at the stages indicated and fixed overnight at 4°C in 4% paraformaldehyde (PFA) in phosphate-buffered saline (PBS). For cryosectioning embryos were washed briefly in PBS, and then passed through a sucrose gradient: 30 min in 5% sucrose in PBS, 30 min in 10% sucrose in PBS before being placed in 20% sucrose in PBS overnight at 4°C. Embryos were embedded in OCT compound and stored at −80°C. Sections were cut on a cryostat at varying thicknesses appropriate to the embryonic stage: For E11.5 at 8 μm, for E13.5 at 10 μm, and for E17.5 at 14 μm. For paraffin sectioning E10.5 embryos were paraffin embedded and subsequently 6 μm thick sections were cut.

## H&E Staining

Cryosections were allowed to reach room temperature before the slides were rehydrated by passage through 100% EtOH 3× 5 min then serial passage through 90, 70, 50, and lastly 30% EtOH for a couple of min each. Slides were washed in $H_2O$ and stained in haemotoxylin for 4 min. They were rinsed in $H_2O$ and subsequently differentiated in acid/alcohol for a few seconds. Slides were again rinsed in $H_2O$ then placed in saturated lithium carbonate solution for a few seconds. They were rinsed in $H_2O$, stained in eosin for 2 min and again rinsed in $H_2O$. Slides were dehydrated through 4 changes of 100% ethanol

and passaged 3× through xylene for 5 min each, subsequently mounted in DPX (Cell Path, SEA-1304-00A), coverslipped and allowed to dry overnight.

## lacZ Expression Analysis, Dawson Staining, and Wholemount in situ Hybridisation

Embryos were analysed for *lacZ* expression between E10.5 and E14.5 through staining for β-gal activity as previously described (Mackenzie et al., 1997). Skeletal preparations from E17.5 foetuses were stained simultaneously with Alizarin Red and Alcian Blue (Nagy et al., 2009a,b). Whole-mount *in situ* hybridisation on half heads was performed as previously described (Hecksher-Sørensen et al., 1998). Whole-mount *in situ* hybridisation on E9.5 day embryos was performed as previously described (Pai et al., 2015).

## RNA FISH

RNA FISH was carried out using custom Stellaris® RNA FISH probes designed against nascent *Shh* mRNA as previously described (Williamson et al., 2019). As per manufacturer's instructions[3], paraffin sections from E10.5 embryos were deparaffinised in xylene, hydrated in ethanol and permeabilised in 70% ethanol overnight at 4°C. Slides were incubated in 10 µg/mL proteinase K in PBS for 20 min at 37°C followed by washes in PBS and wash buffer (2× SSC, 10% deionised formamide). *Shh* RNA FISH probes were diluted in Stellaris RNA FISH hybridisation buffer (#SMF-HB1-10) to 125 nM and hybridised to slides overnight in a humidified chamber at 37°C. Slides were washed twice for 30 min in wash buffer (2× SSC, 10% deionised formamide) at 37°C, counterstained with 5 ng/mL DAPI, washed in PBS and mounted in Vectashield (Vector Laboratories). This was performed in triplicate for both wild-type control and $Shh^{\Delta SBE2/\Delta SBE2}$ embryos.

## RNA FISH Image Analysis

Image capture and analysis of RNA FISH was carried out as previously described (Williamson et al., 2019). Images were taken of ventral hypothalamic region, midbrain and non-expressing diencephalic epithelial wall tissue from three control and $Shh^{\Delta SBE2/\Delta SBE2}$ embryos. Two sections of each embryo were captured per tissue. Images were captured as *z* stacks with step size set at 0.2 µm. Hardware control, image capture and analysis were performed using Nikon Nis-Elements software. Images were deconvolved using a calculated point spread function with the constrained iterative algorithm of Volocity (PerkinElmer). Image analysis was carried out using the Quantitation module of Volocity.

## In situ Hybridisation on Cryosections

For *in situ* on cryosections, the protocol was adaped from Lu et al. (2013) as described.

Briefly, *in situ* probes were placed at 37°C for 5 min, added to hybridisation buffer [1× salt (2 M NaCl, 100 mM Tris,

[3] www.biosearchtech.com/stellarisprotocols

65 mM $NaH_2PO_4$, 50 mM $Na_2HPO_4$, and 50 mM EDTA in $ddH_2O$, pH to 7.5], 50% deionised formamide, 10% dextran sulfate, 1 mg/mL yeast RNA, 1× Denhardt's (2% BSA, 2% Ficcoll, and 2% PVP made up to 100 mL with $ddH_2O$) pre-warmed to 65°C and subsequently denatured at 95°C for 2 min. Probes were added to slides, that had been previously allowed to reach room temperature, and placed in a 65°C waterbath overnight in a chamber humidified with 5× SSC/50% formamide. Slides were subject to 3× 30 min washes at 65°C in washing solution (50% formamide, 25 mL 1× SSC and 0.1% Tween 20 made up to 500 mL Milli-Q $H_2O$). Subsequently, slides were washed 2× 30 min in 1× MABT (100 mM maleic acid, 167 mM NaCl in $ddH_2O$, pH 7.5, then 0.1% Tween 20). Slides were blocked in 1× MABT + 2% blocking reagent + 20% heat inactivated sheep serum. A 1/2,500 dilution of anti-DIG antibody (Roche, 1109327490) in 1× MABT + 20% heat inactivated sheep serum was then added and slides were placed in a humified chamber and incubated overnight at room temperature. Slides were washed 5× for 20 min in 1× MABT. They were then washed with NTMT (100 mM NaCl, 50 mM MgCl, 100 mM Tris pH 9.5, and 0.1% Tween 20 made up in $ddH_2O$) for 10 min followed by NTMTL (NTMT + 5 mM Levamisole) for 10 min. Staining solution, NTMTL containing 3.75 µL/mL BCIP (Roche, 11383221001) and 5 µL/mL NBT (Roche, 11383213001), was then added and slides were placed at 37°C to allow colour to develop. Slides were immersed in $H_2O$, air dried and mounted in Prolong gold (Thermo Fisher Scientific, P39634).

## Immunofluorescence

Cryosections were removed from the −80°C freezer and allowed to reach room temperature before being subjected to antigen retrieval using a citric acid solution (10 mM citric acid dissolved in $ddH_2O$, then pH to 6–6.5) at 65°C for 15 min. Subsequently, slides were washed twice for 5 min in PBS then blocked using 10% goat serum in PBT (0.1% Triton-X100 in PBS) for 1 h at room temperature. For PITX2 staining, donkey serum was used. Slides were incubated in primary antibodies diluted in blocking solution overnight at 4°C as follows: rabbit anti-CASP3 (1:500, Abcam, ab49822); mouse anti-COL2A1 (1:400, Santa Cruz, sc-52659); rabbit anti-ISL1 (1:200, Abcam, ab20670); rabbit anti-LHX3 (1:250, Abcam, ab14555); rabbit anti-NKX2-1 (1:250, Abcam, ab76013); rabbit anti-NKX2-2 (1:250, Abcam, ab191077); rabbit anti-NKX6-1 (1:250, Abcam, ab221549); rabbit anti-OLIG2 (1:200, Abcam, ab109186); rabbit anti-oxytocin (1:500, Abcam, ab212193); rabbit anti-PAX6 (1:350, Abcam, ab195045); sheep anti-PITX2 (1:200, R&D, AF7388); rabbit anti-SF1 (1:200, Abcam, ab65815); rabbit anti-TBX3 (1:200, Abcam, ab99302); rabbit anti-TH1 (1:200, Abcam, ab137869); rabbit anti-TCF4 (1:100, Cell Signalling; C48H11); rabbit anti-vasopressin (1:500, Abcam, ab213707). Slides were then washed 3 times for 10 min each in PBT and incubated for 1 h at room temperature with fluorescent secondary antibodies in PBT in the dark, secondaries as follows: goat anti-rabbit 488 (1:500, Thermo Fisher Scientific, A11034); goat anti-mouse 488 (1:500, Thermo Fisher Scientific, A11029); donkey anti-sheep 594 (1:500, Thermo Fisher Scientific, A11016). Slides were then washed 3 times for 10 min each in PBT and subsequently stained with

0.1 μg/mL DAPI in PBS for 10 min, then washed in PBS twice for 5 min each. Lastly, slides were mounted using Prolong Gold (Thermo Fisher Scientific, P39634) and allowed to dry prior to imaging.

# RESULTS

## Loss of SBE2 Enhancer Activity Leads to Reduction in Rostral Diencephalic *Shh* Expression

To examine the role of the SBE2 enhancer during development, this element was deleted using CRISPR/Cas9 (Cong et al., 2013) to remove 1.2 kb (**Supplementary Figures S1A,B**) containing the conserved element. The SBE2 deleted allele, henceforth referred to as $Shh^{\Delta SBE2}$, was crossed to generate homozygous embryos ($Shh^{\Delta SBE2/\Delta SBE2}$) and also crossed to *Shh* null ($Shh^{null}$) mice to generate compound heterozygous embryos ($Shh^{null/\Delta SBE2}$). Loss of the SBE2 enhancer alone had no effect upon survival as the $Shh^{\Delta SBE2/\Delta SBE2}$ mice were viable and fertile, appeared phenotypically normal and at weaning no reduction from the expected number of mutant mice was found. Conversely, no live $Shh^{null/\Delta SBE2}$ offspring were recorded by postnatal (P) 14 days (**Figure 1B**), these compound heterozygous embryos died perinatally failing to survive beyond P4, with the cause of postnatal lethality currently undetermined. Normal ratios were observed at embryonic (E) 17.5 (**Figure 1A**).
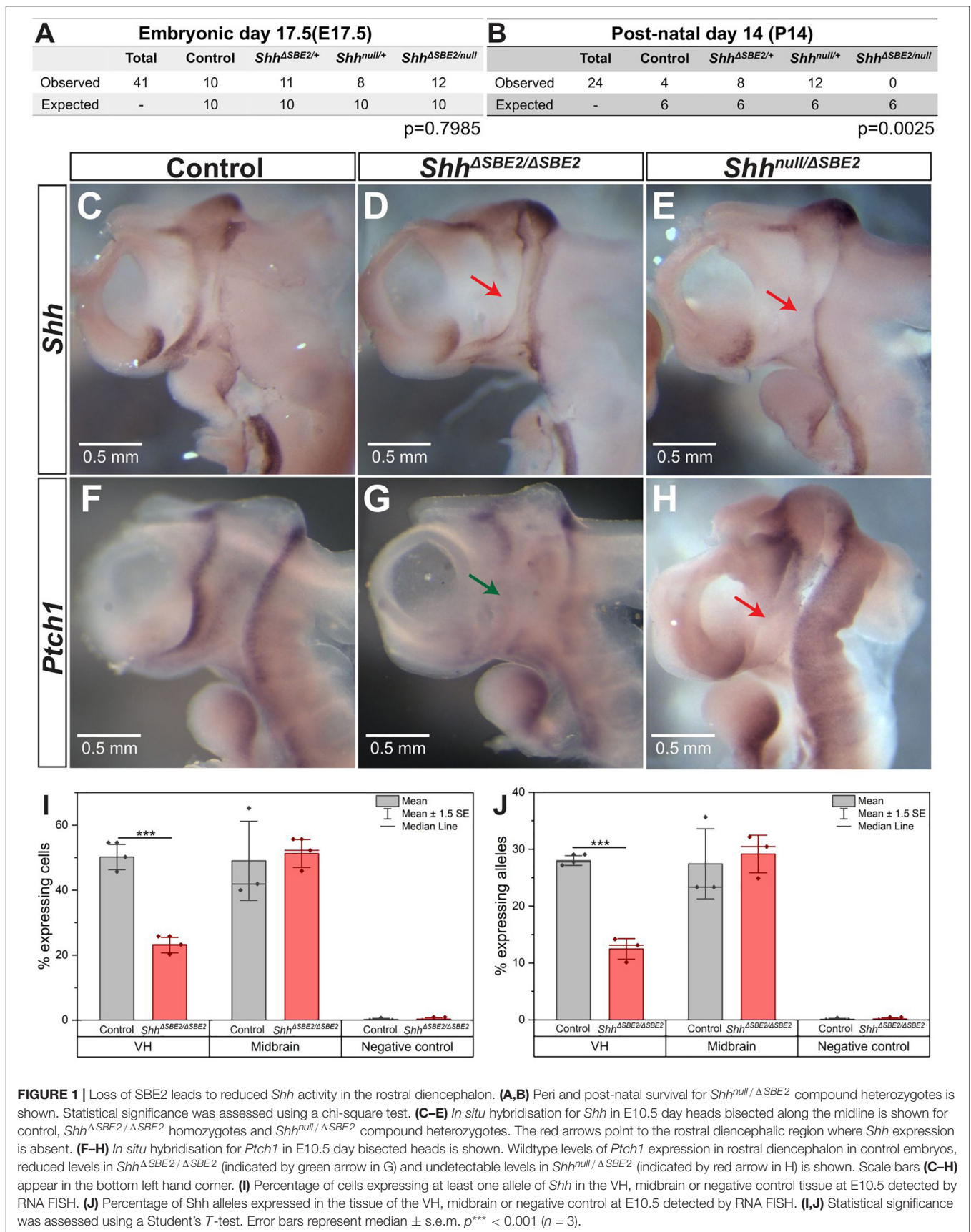
The rostral diencephalon, extending from the ZLI to the MGE, is the target for SBE2 expression as predicted by SBE2/reporter gene analysis in transgenic embryos (Jeong et al., 2006). *Shh* mRNA expression analysis at E10.5 in $Shh^{\Delta SBE2/\Delta SBE2}$ and $Shh^{null/\Delta SBE2}$ embryos revealed levels of *Shh* expression undetected by wholemount *in situ* hybridisation in the ventral portion of the rostral diencephalon in both crosses (**Figures 1C–E** and **Supplementary Figure S2J**). This region of the diencephalon will give rise to the ventral portion of the tuberal and mammillary hypothalamus (Xie and Dorsky, 2017), and for simplicity will henceforth be referred to as the ventral hypothalamus (VH). The region lacking *Shh* expression in the SBE2 mutant embryos, however, was appreciably more restricted than the region predicted by transgenic analysis, this is likely due to overlapping expression caudally directed by other brain enhancers such as SBE3 and SBE4. As compared to wildtype, the $Shh^{null/+}$ embryos showed the same relative pattern of expression, but at a reduced level (Lettice et al., 2014).

The differences in postnatal viability between $Shh^{\Delta SBE2/\Delta SBE2}$ and $Shh^{null/\Delta SBE2}$ suggested that there was residual *Shh* expression in the viable line. Since this residual expression was undetected by *in situ* hybridisation, we used RNA FISH to directly assay transcriptional changes due to the deletion of the SBE2 enhancer. Enhancers regulate the periodicity of transcription affecting the rate of transcriptional bursting (Larsson et al., 2019) and hence, this approach, which assays the production of *Shh* nascent transcripts, provides a relative assessment of enhancer activity. We have previously used RNA FISH to focus on transcriptional changes (Williamson et al., 2019) in small expression domains within embryonic tissues; here,

focusing on expressing cells (**Supplementary Figures S2H,I**) within the VH. In the control VH, about 52% of the cells (**Figure 1I**) exhibited at least one active allele while in the $Shh^{\Delta SBE2/\Delta SBE2}$ mutant, that number was approximately 23% (**Figure 1I**). The majority of actively transcribing cells (∼90%, **Supplementary Figure S2G**) had only a single active allele (**Figure 1J**). Expression of *Shh* is not under SBE2 control in the midbrain and transcriptional differences measured in this region were not significant (**Figures 1I,J**), while non-expressing neighbouring domains showed no appreciable allelic signal (<0.3%). SBE2, therefore, accounted for approximately 55–60% of the transcriptional activity in the VH.

Further reduction in activity in the $Shh^{null/\Delta SBE2}$ embryo was indicated by patched-1 (*Ptch-1*) expression. *Ptch1* expression, which is upregulated by hedgehog signalling and is a sensitive readout of *Shh* expression, was examined at E10.5 (Casillas and Roelink, 2018). Similar to the expression pattern observed for *Shh*, *Ptch1* was also downregulated in the VH upon loss of SBE2 activity (**Figures 1F–H**). However, in this instance, levels differed between the compound heterozygous and the homozygous embryos. While $Shh^{null/\Delta SBE2}$ embryos showed no detectable levels of *Ptch1* expression in the VH (**Figure 1H**, red arrow), the $Shh^{\Delta SBE2/\Delta SBE2}$ embryos presented residual levels (**Figure 1G**, green arrow). It should be noted that while at E9.5 *Shh* levels were low in the ventral diencephalon in the absence of SBE2 for both mutant conditions (**Supplementary Figures S2A–C**), that *Ptch1* expression pattern in neighbouring tissue was comparable to wildtype (**Supplementary Figures S2D–F**). We suggest that *Ptch1* dependent development is unaffected until after E9.5 and the defects occur after this stage. To determine when VH *Shh* expression is downregulated, a mouse line containing the *lacZ* reporter gene inserted into the *Shh* regulatory domain, SBLac526, was used (Anderson et al., 2014) as proxy for *Shh* expression. VH *lacZ* expression was low but detectable up to E13.5 (**Supplementary Figures S3A–C**, red arrow), with expression subsequently absent at E14.5 (**Supplementary Figure S3D**, black arrow). Hence, the effective role of SBE2 encompasses a developmental window that begins sometime after E9.5 extending to E13.5 when all regulatory activity in the VH is decreasing.

The residual levels of *Shh* expression present in the SBE2 mutant appeared capable of rescuing the postnatal lethality. Accordingly, an additional enhancer was identified in *Shh* expressing neural cells from E10.5 dissected heads. ATAC-seq (Buenrostro et al., 2015) revealed a peak corresponding to SBE2, as expected, and additionally a peak at a vertebrate conserved sequence element (position chr5:29230287-29230750 [mm9]) (**Supplementary Figure S4A**), no peaks were detected for SBE3 or SBE4, likely due to the low contribution of the telencephalic cells vs. other brain regions. When used in reporter constructs in transgenic embryos at E10.5 (**Supplementary Figures S4B–D**) the conserved sequence element showed broad expression activity extending anteriorly from the midbrain into the diencephalon (**Supplementary Figures S4B–D**). Recently, an enhancer whose primary function is to drive expression initially in the prechordal plate, and later throughout the ventral forebrain, called SBE7 (Sagai et al., 2019), was reported at the same chromosomal position. Thus, SBE7 has a primary

**A**

### Embryonic day 17.5 (E17.5)

| | Total | Control | $Shh^{\Delta SBE2/+}$ | $Shh^{null/+}$ | $Shh^{\Delta SBE2/null}$ |
|---|---|---|---|---|---|
| Observed | 41 | 10 | 11 | 8 | 12 |
| Expected | - | 10 | 10 | 10 | 10 |

p=0.7985

**B**

### Post-natal day 14 (P14)

| | Total | Control | $Shh^{\Delta SBE2/+}$ | $Shh^{null/+}$ | $Shh^{\Delta SBE2/null}$ |
|---|---|---|---|---|---|
| Observed | 24 | 4 | 8 | 12 | 0 |
| Expected | - | 6 | 6 | 6 | 6 |

p=0.0025



FIGURE 1 | Loss of SBE2 leads to reduced *Shh* activity in the rostral diencephalon. **(A,B)** Peri and post-natal survival for $Shh^{null/\Delta SBE2}$ compound heterozygotes is shown. Statistical significance was assessed using a chi-square test. **(C–E)** *In situ* hybridisation for *Shh* in E10.5 day heads bisected along the midline is shown for control, $Shh^{\Delta SBE2/\Delta SBE2}$ homozygotes and $Shh^{null/\Delta SBE2}$ compound heterozygotes. The red arrows point to the rostral diencephalic region where *Shh* expression is absent. **(F–H)** *In situ* hybridisation for *Ptch1* in E10.5 day bisected heads is shown. Wildtype levels of *Ptch1* expression in rostral diencephalon in control embryos, reduced levels in $Shh^{\Delta SBE2/\Delta SBE2}$ (indicated by green arrow in G) and undetectable levels in $Shh^{null/\Delta SBE2}$ (indicated by red arrow in H) is shown. Scale bars **(C–H)** appear in the bottom left hand corner. **(I)** Percentage of cells expressing at least one allele of *Shh* in the VH, midbrain or negative control tissue at E10.5 detected by RNA FISH. **(J)** Percentage of Shh alleles expressed in the tissue of the VH, midbrain or negative control at E10.5 detected by RNA FISH. **(I,J)** Statistical significance was assessed using a Student's *T*-test. Error bars represent median ± s.e.m. $p^{***} < 0.001$ ($n = 3$).

function in the prechordal plate but, either singly or with other unidentified elements, accounts for approximately 40–45% of the transcriptional activity in the VH. Compensation by *de novo* activation of other *Hh* genes, however, cannot be ruled out.

## Loss of SBE2 Activity Effects Midline Craniofacial Malformations

SBE2 deletion embryos were analysed for craniofacial malformations. Unsurprisingly, given the postnatal viability of $Shh^{\Delta SBE2/\Delta SBE2}$ embryos, no gross craniofacial malformations nor that of the craniofacial skeletal elements (**Supplementary Figures S5A,B**) were observed. In contrast, at E17.5, $Shh^{null/\Delta SBE2}$ embryos exhibited external head malfomation, in which the mutant embryos presented with a more rounded head (**Supplementary Figures S6A–D**). To investigate these changes in head shape, microCT scans of control and $Shh^{null/\Delta SBE2}$ mutant embryos were subject to geometric morphometric analysis (**Supplementary Figure S7**) to visualise and test for differences between control and mutant embryos. All four possible genotypes, $Shh^{+/+}$, $Shh^{null/+}$, $Shh^{\Delta SBE2/+}$, and $Shh^{null/\Delta SBE2}$ were analysed. For all analyses subsequently presented $Shh^{+/+}$, $Shh^{null/+}$, and $Shh^{\Delta SBE2/+}$ clustered together and were indistinguishable. As such, and also due to the previously established lack of phenotypic effects in $Shh^{null/+}$ (Chiang et al., 1996), all three genotypes were used as a control for morphometric analyses. Centroid size, a proxy of skull scale, revealed that the compound heterozygous mutant embryos tended to have an overall reduction in skull size, though this was not significant (pairwise two-sample Wilcoxon, $p = 0.49$) (**Figure 2A**). However, shape variation was significantly affected by size, as well as genotype and litter provided the best regression fit ($R^2 = 0.83$, ANOVA $p < 0.001$). Principal components of allometry-free shape was also explored. We observed clear, genotype-specific separation of control and mutant mice, with the latter occupying a relatively broader expanse of morphospace (**Figure 2B**). In mutants, Principal Component 1 (54.7%) (**Figure 2B**) describes a reduction in the anteroposterior axis while the mediolateral axis expanded (**Figures 2C–H**). Procrustes variances between control and mutant mice were not significant, however, this was presumably due to limitations in statistical power. Indeed, shape differences described by PC1 were significant (Welch Two Sample $t$-test, $p = 1.5 \times 10^{-4}$). OPT analysis revealed that, in addition to presenting a perturbed overall head structure, $Shh^{null/\Delta SBE2}$ embryos displayed affected nasal cavities (**Figures 2J,L**), which were reduced in length. Moreover, a region of brain tissue, specifically the midline hypothalamic tissue, was absent in the mutant embryos (**Figures 2I,K**).

$Shh^{null/\Delta SBE2}$ embryos displayed midline craniofacial bone malformations with a high degree of variability, which, based on phenotypic severity, were classified into three categories: mild, moderate and severe (**Figures 3A–D**). All mutant embryos showed a reduction in the basisphenoid bone, ranging from the presence of only a small remnant (**Figure 3B**, pale green arrow) to complete loss (**Figures 3C,D**) and in the vomer bone, ranging from an excessive fusion (**Figure 3B**, yellow arrow) to complete absence (**Figures 3C,D**). In addition, the moderate and severe

embryos displayed defects in the pterygoid and maxillary bones (**Figures 3C,D**, white and black arrows). Notably, all embryos showed some degree of midline craniofacial malformation, which indicates that *Shh* signalling directed by SBE2 is involved in the midline development of the craniofacial bones, and parallels the role *Shh* plays in early midline brain development (Chiang et al., 1996; Blaess et al., 2014).

## Mislocalised Pituitary and Loss of SHH signalling Disrupts Craniofacial Development

Closer examination of the heads of mutant compound heterozygous embryos revealed that the basisphenoid bone, the most posterior defective cranial bone, was intercepted by the adenohypophyseal pituitary lobe (labelled AP in **Figures 3E–G**). This lobe of the pituitary was misplaced and formed in a more anterior position, growing within the region where the basisphenoid will form (the basis for the mislocalisation is discussed below). Developmental timing of this event suggests that the adenohypophysis disrupts this region before chondrogenesis initiates, which indicates that the adenohypophyseal tissue likely presents a physical barrier to basisphenoid development. The phenotypic variability may correlate with the extent to which the pituitary lobe intercepted the basisphenoid bone in the mutant embryos.
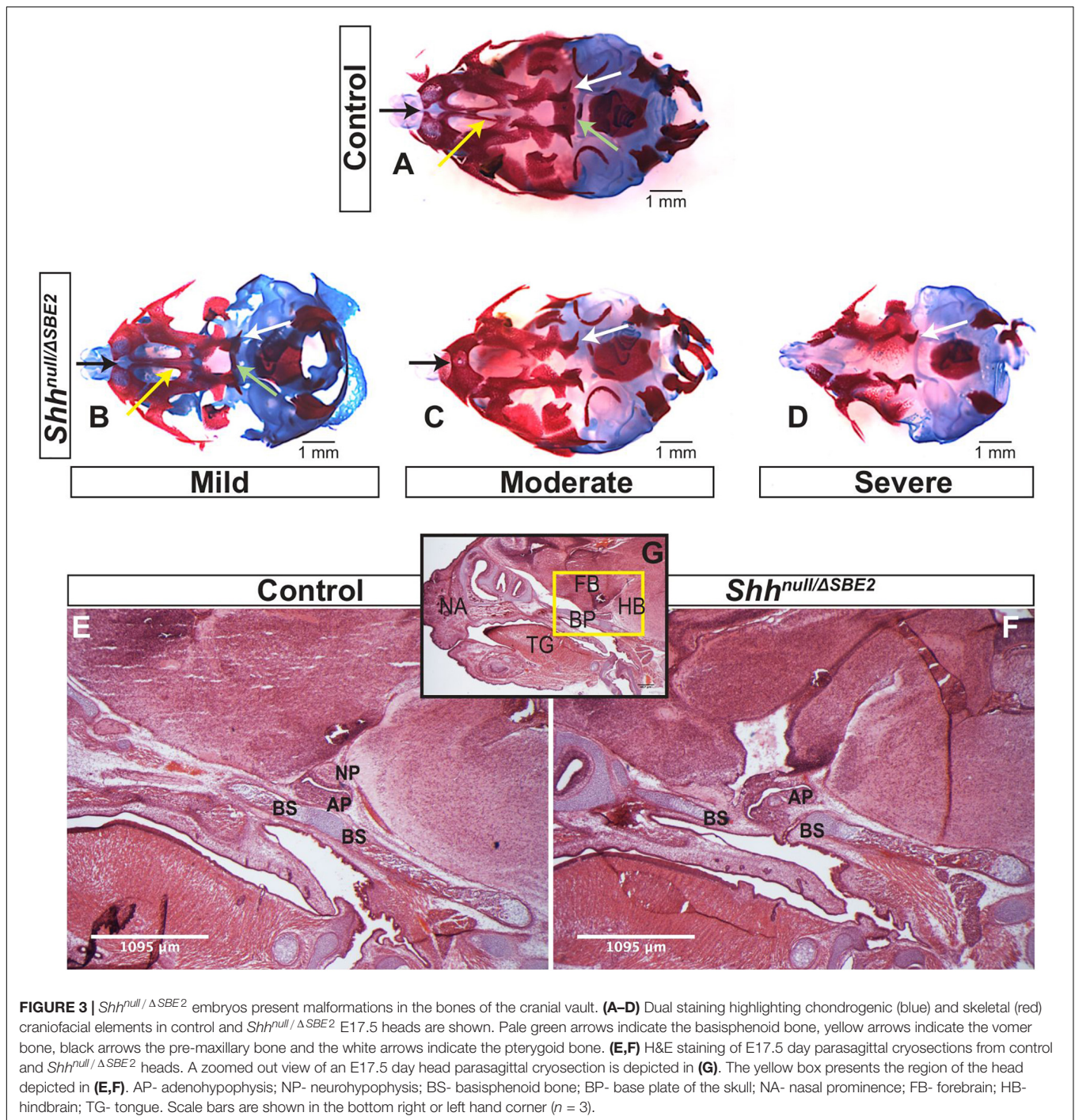
Further investigations into the effect of SBE2 directed expression on craniofacial development focused on mesenchymal *Ptch1* expression in the vicinity of the forebrain. In control embryos at E12.5, *Ptch1* expression was detected within a narrow layer of mesenchyme located directly adjacent to the floor of the diencephalon where *Shh* was expressed (**Figures 4A,B**). COL2A1, a type 2 collagen, is expressed during early cartilage formation (Hissnauer et al., 2010) and co-localised with *Ptch1* in control embryos (**Figures 4E,F**), indicating that the underlying facial mesenchyme is under the influence of SHH and is committed toward cartilage formation. At the same stage in the $Shh^{null/\Delta SBE2}$ embryos, *Ptch1* expression was reduced in the underlying mesenchyme (**Figures 4C,D**) and only a thin lining of cells expressing COL2A1 was seen (**Figures 4G,H**). The loss of *Ptch1* and COL2A1 staining was found to be independent of the physical disruptive effects caused by mislocalisation of the adenohypophysis, as the absence of both markers was evident in regions of the cranial base which lie anterior to disrupted adenohypophyseal tissue detected in the mutant embryos (**Figures 4C,G**). Thus, SBE2 mediated *Shh* expression contributed to an adequate cell response and bone formation in the sub–diencephalic mesenchyme along the midline of the palatal floor, and reduction of this cell population is critical for the midline craniofacial phenotype.

## $Shh^{null/\Delta SBE2}$ Embryos Display Mislocalised and Deformed Pituitary Lobes Due to Disruption of the AP Hypothalamic Boundary

Pituitary lobe development was analysed at stages E11.5, E13.5, E15.5, and E17.5. In $Shh^{null/\Delta SBE2}$ mutant embryos
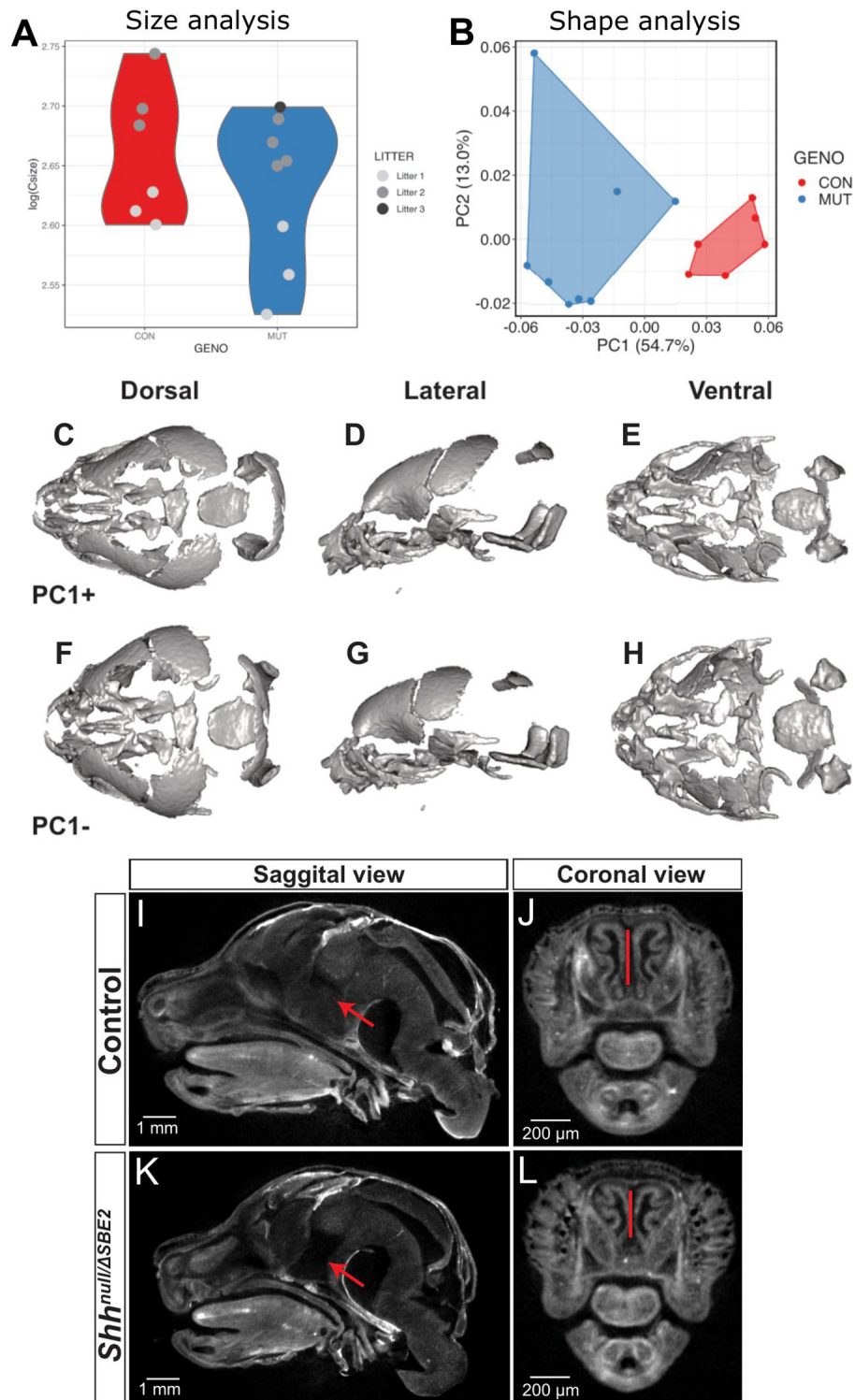
**FIGURE 2 |** $Shh^{null/\Delta SBE2}$ embryos have an altered head shape and gross malformations. **(A)** Skull size, as described by the log(centroid size) landmark configurations of control and $Shh^{null/\Delta SBE2}$ at E17.5. **(B)** Principal components (PC) plot of allometry-free skull shape at E17.5. **(C–H)** Dorsal, lateral and ventral views of a mean surface warped according to extreme positive PC1 **(C–E)** or negative PC1 **(F–H)** (control $n = 6$; mutant $n = 8$). **(I–L)** OPT scan stills from E17.5 day control and $Shh^{null/\Delta SBE2}$ heads, presenting the midline sagittal plane and the coronal nasal region. Red arrows point to the region of hypothalamic tissue which is absent in $Shh^{null/\Delta SBE2}$ embryos. Red lines serve to demonstrate the reduced nasal cavities found in $Shh^{null/\Delta SBE2}$ embryos. Scale bars are depicted in the bottom left hand corner (control $n = 2$; mutant $n = 3$).

**FIGURE 3** | $Shh^{null/\Delta SBE2}$ embryos present malformations in the bones of the cranial vault. **(A–D)** Dual staining highlighting chondrogenic (blue) and skeletal (red) craniofacial elements in control and $Shh^{null/\Delta SBE2}$ E17.5 heads are shown. Pale green arrows indicate the basisphenoid bone, yellow arrows indicate the vomer bone, black arrows the pre-maxillary bone and the white arrows indicate the pterygoid bone. **(E,F)** H&E staining of E17.5 day parasagittal cryosections from control and $Shh^{null/\Delta SBE2}$ heads. A zoomed out view of an E17.5 day head parasagittal cryosection is depicted in **(G)**. The yellow box presents the region of the head depicted in **(E,F)**. AP- adenohypophysis; NP- neurohypophysis; BS- basisphenoid bone; BP- base plate of the skull; NA- nasal prominence; FB- forebrain; HB-hindbrain; TG- tongue. Scale bars are shown in the bottom right or left hand corner ($n = 3$).

at E11.5, Rathke's pouch (RP), which will give rise to the adenohypophyseal lobe, and the infundibulum, which will give rise to the neurohypophyseal pituitary lobe, were both ectopically shifted ventrally (**Supplementary Figures S8A,B**). These findings reflect the previous observations by Zhao et al. (2012) using conditional *Shh* deletion mice. At E13.5, RP was severely malformed in the $Shh^{null/\Delta SBE2}$ mutant embryos, while the infundibulum did not separate from the neuroectodermal tissue to the same degree as control counterparts (**Figures 5A–C**)

and remained ectopically located at E15.5 (**Supplementary Figures S8C,D**). Interestingly, at E17.5 the neurophypophysis appeared absent in the $Shh^{null/\Delta SBE2}$ mutant embryos (**Figures 3E,F**), yet staining for markers of neurohypophyseal tissue revealed that this was due to the lack of separation of the neurohypophyseal tissue from the neuroectodermal tissue of origin (**Figures 5L,N**). Moreover, caspase-3 (CASP3) staining revealed that this remnant neurohypophyseal tissue appeared to be undergoing apoptosis (**Figures 5M,O**) indicating that
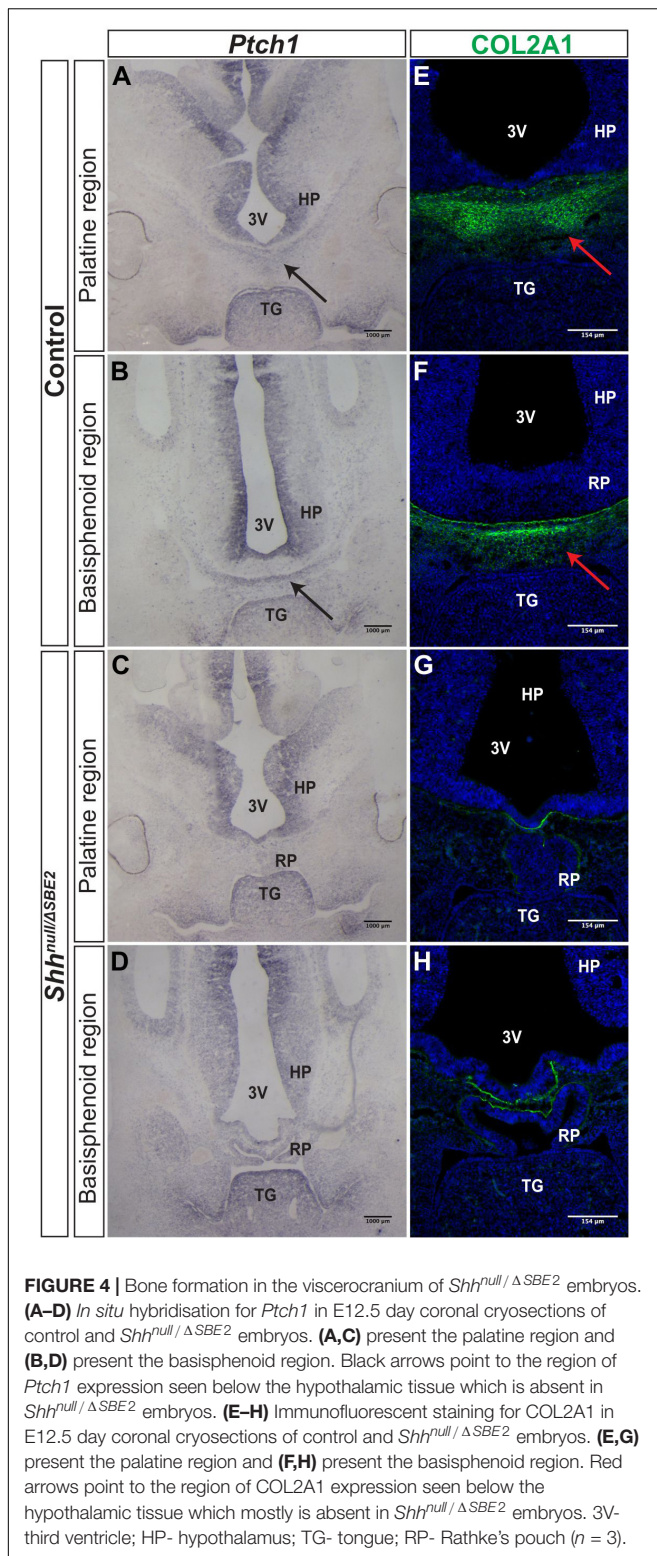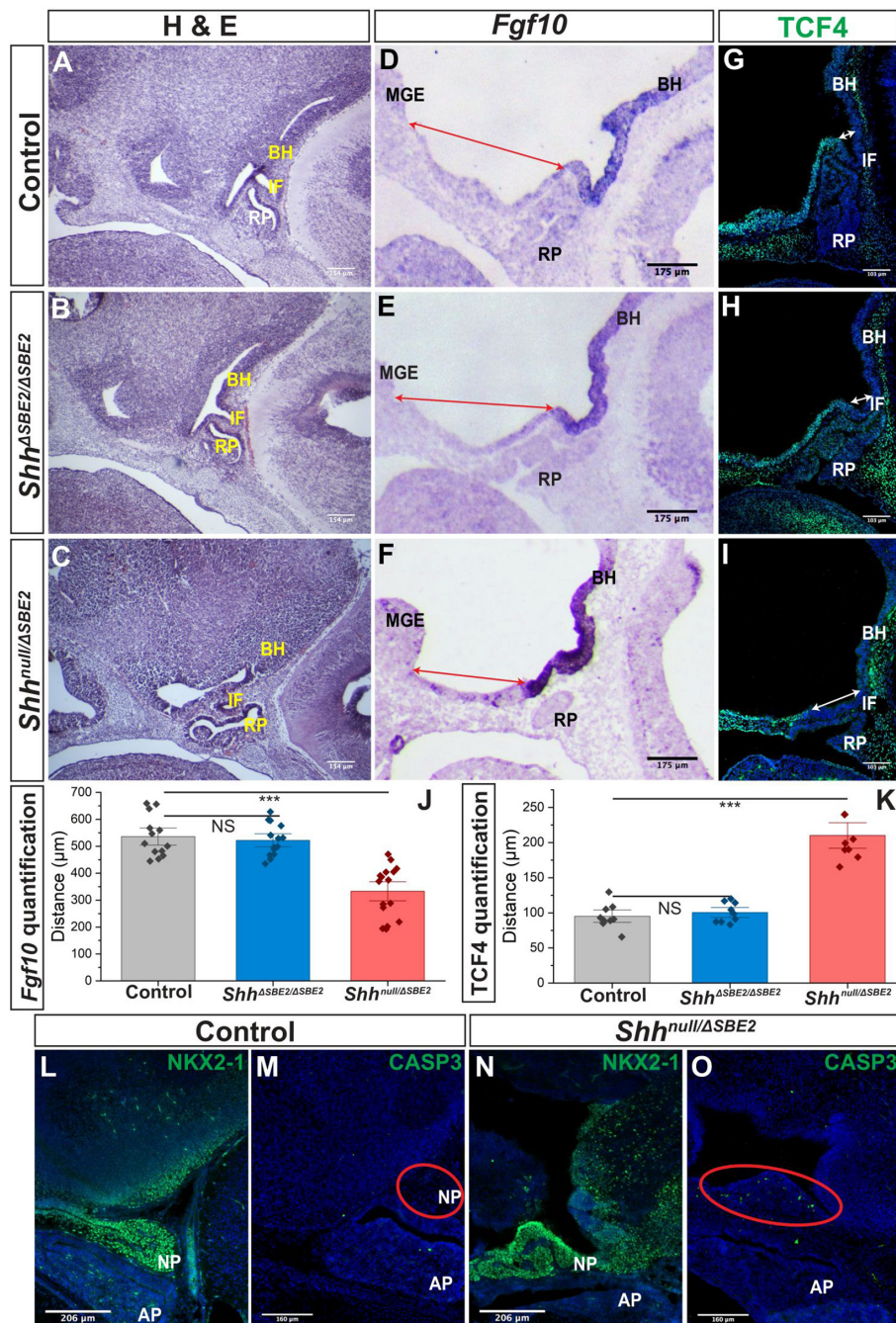
**FIGURE 4 |** Bone formation in the viscerocranium of $Shh^{null/\Delta SBE2}$ embryos. **(A–D)** In situ hybridisation for Ptch1 in E12.5 day coronal cryosections of control and $Shh^{null/\Delta SBE2}$ embryos. **(A,C)** present the palatine region and **(B,D)** present the basisphenoid region. Black arrows point to the region of Ptch1 expression seen below the hypothalamic tissue which is absent in $Shh^{null/\Delta SBE2}$ embryos. **(E–H)** Immunofluorescent staining for COL2A1 in E12.5 day coronal cryosections of control and $Shh^{null/\Delta SBE2}$ embryos. **(E,G)** present the palatine region and **(F,H)** present the basisphenoid region. Red arrows point to the region of COL2A1 expression seen below the hypothalamic tissue which mostly is absent in $Shh^{null/\Delta SBE2}$ embryos. 3V-third ventricle; HP- hypothalamus; TG- tongue; RP- Rathke's pouch (n = 3).

To exclude the possibility that the observed pituitary malformation and mislocalisation were due to a developmental delay, expression of adenohypophyseal markers that display stage-specific restricted expression were analysed. ISL1 is expressed throughout the early developing adenohypophysis but later becomes restricted to the ventral most portion of the lobe (Ericson et al., 1998; Castinetti et al., 2015). This same restriction of expression is seen for TBX3, which is expressed broadly throughout the developing adenohypophysis, but by E12.5 expression is restricted to the ventral aspect of the lobe (Pontecorvi et al., 2008). For both ISL1 (**Supplementary Figures S10A,B**) and TBX3 (**Supplementary Figures S10C,D**) expression in the adenohypophysis at E12.5 in $Shh^{null/\Delta SBE2}$ embryos was found to reflect the pattern seen in control embryos, with expression only detected in the ventral most portion, indicating that the adenohypophyseal lobe was not developmentally delayed.

While patterning and early neuronal marker expression within the pituitary lobes appeared normal, at later developmental stages, E17.5, neuronal populations within varied nuclei of the VH, which establish connections with the pituitary lobes, were disrupted. Both the tyrosine hydroxylase (TH1) (**Supplementary Figures S11A,B**) and the vasopressin neuronal population (**Supplementary Figures S11E,F**) of the paraventricular nucleus (PVN) were lost in $Shh^{null/\Delta SBE2}$ embryos. Additionally, the oxytocin neuronal population of the PVN was absent while the population found within the arcuate nucleus (ARC) was either misspecified or mislocalised (**Supplementary Figures S11C,D**). To confirm that the loss of PVN and ARC neuronal populations did not result from a developmental delay in hypothalamic neuronal specification, expression of oxytocin and TH1 was analysed at E15.5. At E15.5 oxytocin expression was present in the PVN of the control embryos (**Supplementary Figure S12A**, white arrow) but absent from $Shh^{null/\Delta SBE2}$ embryos (**Supplementary Figure S12B**). Similarly, expression of TH1 was detected in the ARC of control embryos (**Supplementary Figure S12C**, yellow arrow), yet no expression was detected in $Shh^{null/\Delta SBE2}$ embryos (**Supplementary Figure S12D**). This indicates that the lack of specific gene expression in hypothalamic neuronal populations at E15.5 persists for at least two additional days up to E17.5, arguing for a loss of the neuronal population and not a developmental delay in neuronal specification. These results indicate that, in addition to the disruption of hypophyseal structure and location in development, there is also disruption of hypothalamic neuronal populations, demonstrating that SBE2 activity contributes to the role of Shh in hypophyseal and hypothalamic neuronal development. Interestingly, the hypothalamic populations found to be affected are known to establish connections with and regulate the hypophysis, indicating that Shh plays a role in coordinating hypophyseal development and subsequent neuronal regulation. The disruption of these late neuronal populations in $Shh^{null/\Delta SBE2}$ embryos revealed that early loss of SBE2 directed Shh activity in the VH has late effects upon development in the hypothalamus, at timepoints at which Shh expression is no longer present in the tissue in question (**Supplementary Figure S3**).

inadequate neurohypophyseal partitioning likely led to tissue degeneration. Despite the fact that both hypophyseal lobes were misspecified in the $Shh^{null/\Delta SBE2}$ embryos, early hypophyseal patterning was unperturbed (**Supplementary Figures S9C,F,I,L**).

**FIGURE 5 |** The AP hypothalamic boundary is shifted ventrally in $Shh^{null/\Delta SBE2}$ embryos. **(A–C)** H&E staining of E13.5 day sagittal cryosections of control, $Shh^{\Delta SBE2/\Delta SBE2}$ and $Shh^{null/\Delta SBE2}$ embryos. **(D–F)** In situ hybridisation for Fgf10 in E11.5 day sagittal cryosections of control, $Shh^{\Delta SBE2/\Delta SBE2}$ and $Shh^{null/\Delta SBE2}$ embryos. Red arrows represent the distance between the MGE and the anterior boundary of Fgf10 expression. **(G–I)** Immunofluorescent staining for TCF4 in E11.5 day sagittal cryosections of control, $Shh^{\Delta SBE2/\Delta SBE2}$ and $Shh^{null/\Delta SBE2}$ embryos. White arrows represent the distance between the posterior infundibulum and the posterior boundary of TCF4 expression. **(J)** Image J measurement based quantification of the distance (in μm) depicted by the red arrows in **(D–F)** in control, $Shh^{\Delta SBE2/\Delta SBE2}$ and $Shh^{null/\Delta SBE2}$ embryos. Statistical significance was assessed using the Student's T-test. Error bars represent median ± s.e.m. ***$p < 0.001$. **(K)** Image J measurement based quantification of the distance (in μm) between depicted by the white arrows in **(G–I)** in control, $Shh^{\Delta SBE2/\Delta SBE2}$ and $Shh^{null/\Delta SBE2}$ embryos. Statistical significance was assessed using the Student's T-test. Error bars represent median ± S.E.M. ***$p < 0.001$. **(L,N)** Immunofluorescent staining for NKX2-1 in E17.5 day sagittal cryosections of control and $Shh^{null/\Delta SBE2}$ embryos. **(M,O)** Immunofluorescent staining for CASP3 in E17.5 day sagittal cryosections of control and $Shh^{null/\Delta SBE2}$ embryos. Red circles demarcate the region of cell death apparent in mutant embryos. NS, not significant; BH, basal hypothalamus; IF, infundibulum; RP, Rathke's pouch; MGE, medial ganglionic eminence. Scale bars are shown in the bottom left hand corner ($n = 3$).

In $Shh^{\Delta SBE2/\Delta SBE2}$ mutant embryos, neither the adenohypophysis nor the neurohypophysis were ectopically located and both lobes had separated from the tissue of origin at E13.5 (**Supplementary Figure S5**). Additionally, no defects were observed in early marker expression (**Supplementary Figures S9B,E,H,K**); however, mild malformations were detected predominantly in the structure of the lateral portion of adenohypophyseal lobe in $Shh^{\Delta SBE2/\Delta SBE2}$ mutant embryos (**Supplementary Figures S5C–K**).

Distinct anterior-posterior expression domains are established along the midline of the hypothalamus by E9.5. The posterior hypothalamic domain expresses factors including *Bmp4* and *Fgf10* whilst the anterior domain expresses *Six6*, *Tcf4,* and *Shh*. Mutual inhibition between these two gene expression domains exists, whereby in the absence of one domain the opposing domain will expand to occupy the hypothalamic space (Ericson et al., 1998; Takuma et al., 1998). The infundibulum expresses the posterior markers *Bmp4* and *Fgf10* and is specified dorsally to the anterior hypothalamic tissue, at the AP transition zone (Ferrand, 1972; Kawamura and Kikuyama, 1995; Takuma et al., 1998; Treier et al., 1998). Inductive cues from the ventral hypothalamic tissue play a role in orchestrating the formation of RP (Schwind, 1928; Takuma et al., 1998). As RP and the infundibulum were both shifted ventrally in the $Shh^{null/\Delta SBE2}$ mutant embryos (**Figure 5C**), verification of any other associated defects in the establishment of the AP hypothalamic boundary were sought. The posterior boundary of expression of TCF4 was shifted ventrally in the mutant embryos (**Figures 5G–I**) whereas the anterior boundary of expression of *Fgf10* was shifted ventrally, expanding expression (**Figures 5D–F**). Using ImageJ based measurements, the distance (in $\mu$m) between the boundaries of expression and known landmarks was assessed and the shift observed for both the anterior and posterior markers was found to be significant in the $Shh^{null/\Delta SBE2}$ mutant embryos (**Figures 5J,K**). These results indicated that there is a shift in the AP domain boundary with a reduction in anterior markers and gain of posterior markers. In the $Shh^{\Delta SBE2/\Delta SBE2}$ mutant embryos no shift in expression of TCF4 (**Figure 5H**) or *Fgf10* (**Figure 5E**) was observed, correlating with correct positioning of the pituitary lobes (**Figure 5C**). These results suggest that shift of the pituitary lobes occurs as a result of the aberrant specification of the AP boundary, which does not appear to be sensitive to reduced levels of SHH found in $Shh^{\Delta SBE2/\Delta SBE2}$ embryos (**Supplementary Figures S5C–F**).

## Loss of SBE2 Enhancer Activity Leads to Defects in Hypothalamic Patterning in a Concentration Dependent Manner

Much of our knowledge about DV hypothalamic patterning is informed by what is known regarding DV neural tube patterning. In the developing neural tube, neural progenitors acquire distinct transcriptional identities based on length of exposure to patterning signals and DV positioning (Dessaud et al., 2007, 2010; Balaskas et al., 2012). Indeed it is the opposing action of the dorsal neural tube signals *Wnts* and BMPs and the ventral neural tube signal *Shh* that drive patterning along this axis (Burbridge et al., 2016). Subsequently, expression of distinct combinations of transcription factors drives the differentiation of the neural progenitors toward specific neural fates (Dessaud et al., 2008). In the developing hypothalamus *Shh* is initially expressed from the prechordal mesoderm; it is subsequently expressed along the floor plate and plays a role in inducing ventral hypothalamic fate (Burbridge et al., 2016; Corman et al., 2018). In contrast, BMPs are expressed from the roof of the telencephalon, regulating alar hypothalamic development (Burbridge et al., 2016). Given that *Shh* signalling from the hypothalamic floor plate was reduced in the $Shh^{\Delta SBE2/\Delta SBE2}$ and $Shh^{null/\Delta SBE2}$ mutant embryos, DV hypothalamic patterning was examined. Genes whose expression are responsive to SHH levels in the neural tube were of particular interest. No differences were detected between wild-type, $Shh^{\Delta SBE2/+}$ and $Shh^{null/+}$ embryos (**Supplementary Figure S13**), indicating that heterozygous loss of *Shh* has no effect upon DV patterning marker expression.

Expression of PAX6, known to be expressed within the alar hypothalamus, and the opposing basal hypothalamic marker NKX2-2 (Guillemot, 2007; Croizier et al., 2015) were examined. NKX2-2 expression commences early in hypothalamic development, with expression detected in the basal hypothalamic region which borders the alar zone. Later in development, this expression pattern alters within the VH, whereby expression has forked into two bilateral stripes; one that occupies the transition zone of the alar-basal hypothalamus extending into the alar hypothalamus itself, and a second stripe that resides within the basal hypothalamic territory of the VH (Burbridge et al., 2016). At E13.5, this bilateral stripe expression pattern was observed in control embryos (**Figure 6A**). However, in $Shh^{\Delta SBE2/\Delta SBE2}$ mutants the dorsal VH stripe, within the basal hypothalamus, presented patchy expression (**Figure 6B**). The $Shh^{null/\Delta SBE2}$ mutant embryos were more severely affected, with both the alar and basal VH stripes absent (**Figure 6C**). This data indicate that low levels of *Shh* expression can induce some NKX2-2 expression in $Shh^{\Delta SBE2/\Delta SBE2}$, however, these low levels are not sufficient to either specify or maintain the entirety of the NKX2-2 population.

PAX6 is a neural tube and hypothalamic marker, whose expression pattern is known to be restricted to the alar hypothalamus (Burbridge et al., 2016) and, as expected, E13.5 control embryos displayed PAX6 expression solely within the alar portion of the VH (**Figure 6D**). In $Shh^{\Delta SBE2/\Delta SBE2}$ mutant embryos there was a dorsal expansion of PAX6 expression into the basal hypothalamic region in the embryos (**Figure 6E**). In $Shh^{null/\Delta SBE2}$ embryos, this dorsal expansion of PAX6 expression was more severe, with large patches of PAX6 expression detected in the basal hypothalamus of the mutant embryos (**Figure 6F**). These results indicate that *Shh* signalling from the basal hypothalamus is required to restrict PAX6 expression solely to the alar region, and that low levels of *Shh* activity, those found in basal hypothalamus of $Shh^{\Delta SBE2/\Delta SBE2}$ mutants, are not sufficient to exclude PAX6 activity from this region.

These results for NKX2-2 and PAX6 within the VH, upon loss of SHH signalling activity, mirror what was found by Corman et al. (2018). However, these data demonstrate a novel dose dependent effect of SHH signalling whereby these transcription factors are not only able to respond to the presence, or indeed
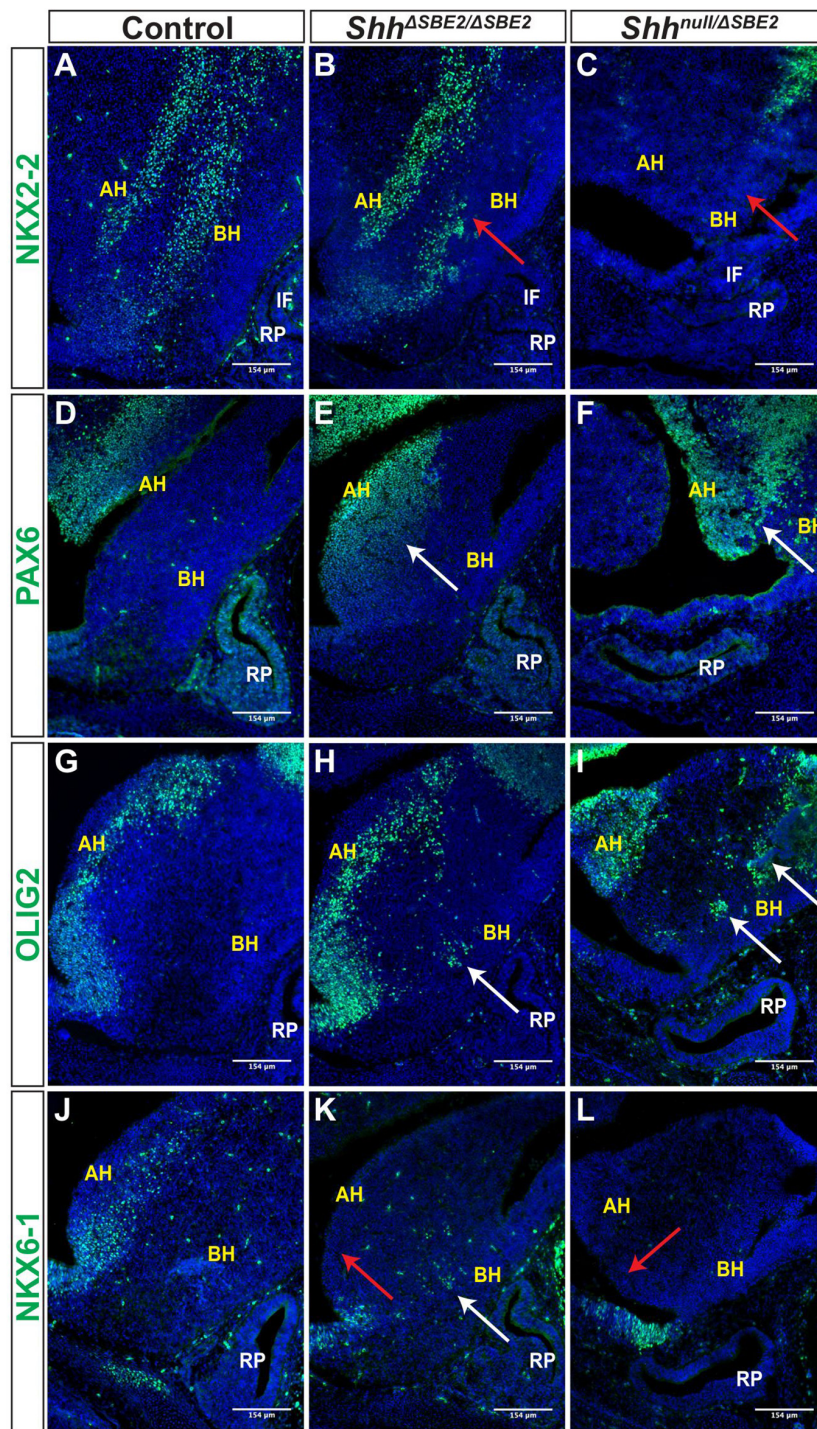
**FIGURE 6 |** DV hypothalamic patterning is affected by loss of SBE2. **(A–C)** Immunofluorescent staining for NKX2-2 in E13.5 day ventral hypothalamic (VH) parasagittal cryosections of control, $Shh^{\Delta SBE2/\Delta SBE2}$ and $Shh^{null/\Delta SBE2}$ embryos. Red arrows point to the region of NKX2-2 expression in the basal hypothalamus which is reduced or absent upon removal of SBE2 enhancer function. **(D–F)** Immunofluorescent staining for PAX6 in E13.5 day VH parasagittal cryosections of control, $Shh^{\Delta SBE2/\Delta SBE2}$ and $Shh^{null/\Delta SBE2}$ embryos. White arrows point to the region of ectopic PAX6 expression in the BH which is seen upon removal of SBE2 function. **(G–I)** Immunofluorescent staining for OLIG2 in E13.5 day VH parasagittal cryosections of control, $Shh^{\Delta SBE2/\Delta SBE2}$ and $Shh^{null/\Delta SBE2}$ embryos. White arrows point to the ectopic regions of expression of OLIG2 in the BH which are seen upon removal of SBE2 function. **(J–L)** Immunofluorescent staining for NKX6-1 in E13.5 day VH parasagittal cryosections of control, $Shh^{\Delta SBE2/\Delta SBE2}$ and $Shh^{null/\Delta SBE2}$ embryos. Red arrows point to the region of NKX6-1 expression in the AH which is absent upon removal of SBE2 function whilst white arrows point to the region of ectopic expression in the BH seen in $Shh^{\Delta SBE2/\Delta SBE2}$ embryos. AH- alar hypothalamus; BH- basal hypothalamus; IF- infundibulum; RP- Rathke's pouch. Scale bars are shown in the bottom right hand corner ($n = 3$).

absence, of *Shh* signalling, but are also sensitive to the amount of *Shh*, with the levels of *Shh* activity being key for the establishment of hypothalamic signalling domains.

Expression of the transcription factor OLIG2 is induced by SHH (Dessaud et al., 2008), and in control embryos was detected in the alar hypothalamus in a narrow region along the edge of the third ventricle (**Figure 6G**). In $Shh^{\Delta SBE2/\Delta SBE2}$ mutant embryos, however, the OLIG2 positive cells showed a subtle dorsal shift away from the edge of the third ventricle and additional expressing cells were detected in the basal hypothalamus (**Figure 6H**). In $Shh^{null/\Delta SBE2}$ mutant embryos, OLIG2 positive staining cells had dramatically shifted into the basal portion of the hypothalamus, with large areas of positive staining cells detected (**Figure 6I**). These data indicated that *Shh* activity acts to ensure adequate OLIG2 expression within the alar hypothalamus, whereupon reduction of SHH allows for OLIG2 expression within the basal hypothalamus. Unexpectedly, OLIG2 was found to be expanded into ectopic regions of the VH in mutant embryos rather than gradually reduced with increasing loss of SHH activity. However, Balaskas et al., 2012, demonstrated in the neural tube that, whilst NKX2-2 and OLIG2 are both equally responsive to SHH activity, higher levels of signalling are required for NKX2-2 expression as it is repressed by both PAX6 and OLIG2, creating a gene regulatory network between these three transcription factors. Thus, in this instance, the residual levels of *Shh* expression directed by SBE7 in $Shh^{null/\Delta SBE2}$ mutant embryos are likely sufficient to induce OLIG2 expression, yet not NKX2-2 due to the repressive activity of OLIG2 and PAX6.

NKX6-1, another transcription factor induced by SHH in the neural tube (Dessaud et al., 2008), was expressed in the alar hypothalamus in a narrow region along the edge of the third ventricle in sagittal and parasagittal regions (**Figure 6J**); but in contrast to OLIG2, these cells were only detected along the basal lateral edge of the third ventricle. In $Shh^{\Delta SBE2/\Delta SBE2}$ mutant embryos, NKX6-1 expression along the basal lateral edge of the third ventricle was undetectable (**Figure 6K**), however, isolated groups of expressing cells were detected in the basal hypothalamus (**Figure 6K**). $Shh^{null/\Delta SBE2}$ mutants showed complete loss of the region of staining along the basal lateral edge with no additional regions of expression observed (**Figure 6L**). NKX6-1 appears to require low levels of *Shh* expression to be induced, levels which are normally found along the edge of the third ventricle. In $Shh^{\Delta SBE2/\Delta SBE2}$ mutants the levels of *Shh* expression are reduced within the basal hypothalamus to a level that allows for ectopic expression of NKX6-1 within this region. In $Shh^{null/\Delta SBE2}$ mutants the complete loss of the expressing cells from the edge of the third ventricle indicates that the levels of *Shh* signalling activity within the VH, directed by SBE7, are insufficient to induce expression of NKX6-1. These data demonstrate a novel, previously undescribed role for SHH activity in the regulation of NKX6-1 expression within the hypothalamus, which mirrors the role described in the neural tube (Sander et al., 2000). Thus, providing further evidence that the signalling network which operates in the neural tube has been co-opted in hypothalamic development.

For all hypothalamic markers analysed, the extent of changes in expression correlate to the scale of alteration in levels of *Shh*

expression, suggesting that *Shh* signalling is functioning in a concentration dependent manner to induce ventral patterning in the hypothalamus. The data described not only present novel examples of patterning genes regulated by SHH activity, as is the case for NKX6-1, but also expand on data presented by Corman et al. (2018). We further demonstrate that, not only do these genes require SHH activity to be adequately expressed, but they are capable of responding to varying levels of SHH. This concentration dependent effect mirrors that seen for *Shh* in the neural tube, and involves many of the same key players, indicating that *Shh* is acting as a morphogen within the VH to regulate tissue establishment within this critical brain region.

## SBE2 Enhancer Activity Controls Downstream Effects Upon Hypothalamic Neuronal Populations

We next sought to assess the effects of disrupted DV patterning on neuronal populations. We first verified that there were no detectable differences in marker expression between wild-type and heterozygotes, $Shh^{\Delta SBE2/+}$ and $Shh^{null/+}$ embryos (**Supplementary Figure S14**), demonstrating that heterozygous loss of *Shh* has no gross effect upon DV neuronal population specification. To examine the effect of disrupted DV patterning upon the establishment of the different ventral hypothalamic neuronal populations, we first analysed expression of the broad ventral hypothalamic neuronal marker NKX2-1 (Ohyama et al., 2005). In control embryos at E13.5, NKX2-1 positive cells were detected across the entirety of the basal hypothalamic domain (**Figure 7A**). In $Shh^{\Delta SBE2/\Delta SBE2}$ mutant embryos, the region of NKX2-1 expressing cells was reduced and embedded within smaller domains intermingled with patches devoid of staining (**Figure 7B**). In the $Shh^{null/\Delta SBE2}$ mutants the region of expression was further reduced with larger and more numerous patches of negative cells observed (**Figure 7C**). These results indicate that whilst SHH activity is required for proper induction of the NKX2-1 neuronal population, that it is either responsive to very low levels of *Shh* signalling or another factor must also sustain the remnant expression seen in mutant embryos.

ISL1 is a melanocortinogenic neuronal marker, for which positive cells are detected throughout the hypothalamus (Kim et al., 2015). In control embryos positive staining was detected throughout the basal hypothalamic region, as expected (**Figure 7D**). In $Shh^{\Delta SBE2/\Delta SBE2}$ mutant embryos expression within the alar hypothalamus was reduced whilst within the basal hypothalamus it was unaffected (**Figure 7E**), in $Shh^{null/\Delta SBE2}$ mutants there was substantial loss of positive staining cells in both the alar and the basal hypothalamus (**Figure 7F**).

We additionally verified whether neurons that are restricted to specific nuclei of the basal hypothalamus were affected upon removal of SBE2 activity. Steroidogenic factor 1 (SF1) positive neurons are localised to the ventromedial hypothalamus (VMH) and are involved in the regulation of glucose metabolism and energy balance (Choi et al., 2013). In control embryos, as expected, SF1 positive neurons were detected in the developing VMH of the basal hypothalamus (**Figure 7G**). In $Shh^{\Delta SBE2/\Delta SBE2}$ mutant embryos the region of the basal hypothalamus expressing
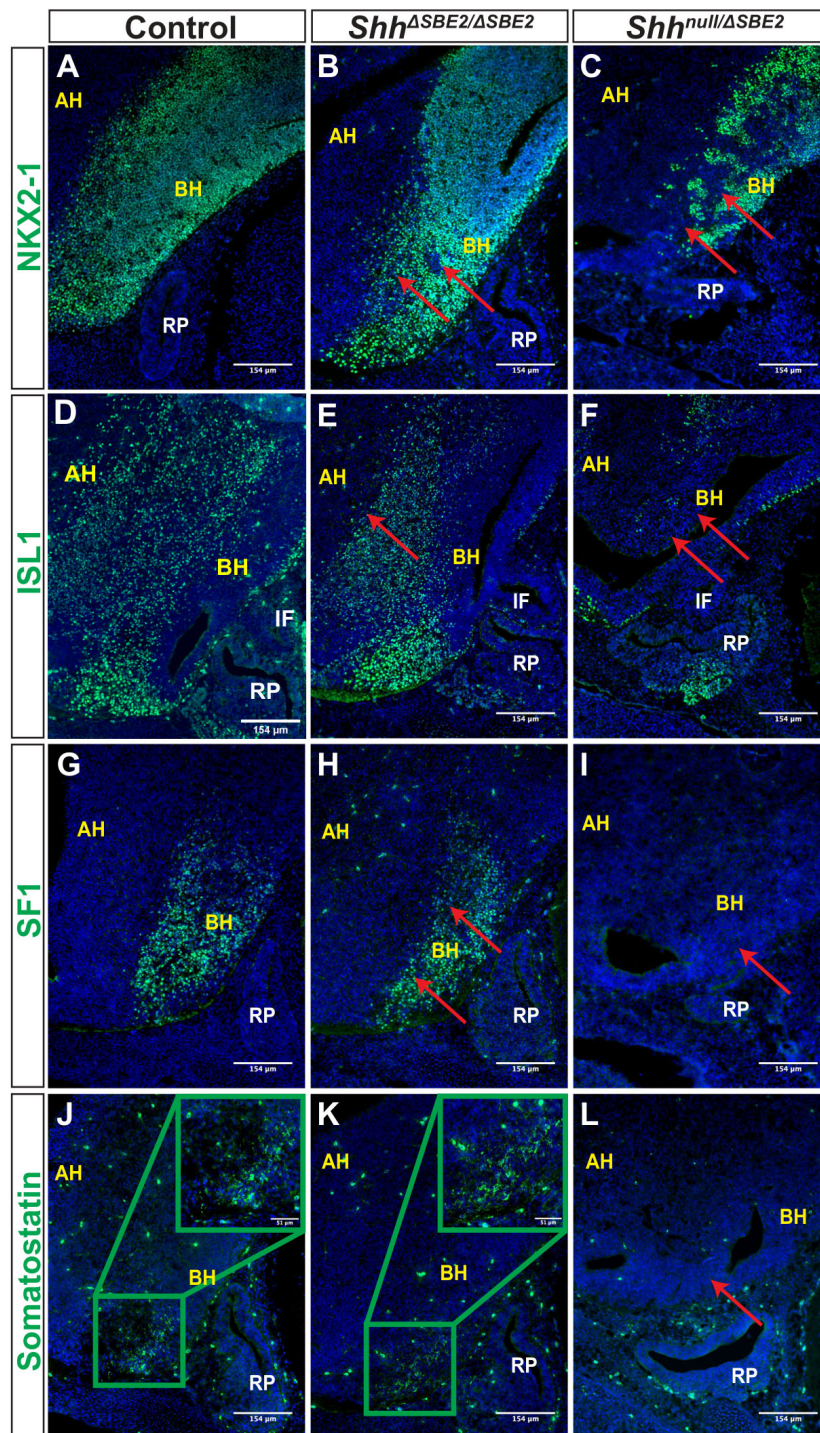
**FIGURE 7 |** DV hypothalamic neuronal populations are affected by loss of SBE2. **(A–C)** Immunofluorescent staining for NKX2-1 in E13.5 day VH parasagittal cryosections of control, $Shh^{\Delta SBE2/\Delta SBE2}$ and $Shh^{null/\Delta SBE2}$ embryos. Red arrows point to the regions devoid of NKX2-1 expression which are found upon removal of SBE2 function. **(D–F)** Immunofluorescent staining for ISL1 in E13.5 day VH parasagittal cryosections of control, $Shh^{\Delta SBE2/\Delta SBE2}$ and $Shh^{null/\Delta SBE2}$ embryos. Red arrows point to the regions of the BH where ISL1 is affected in $Shh^{\Delta SBE2/\Delta SBE2}$ or mostly absent in $Shh^{null/\Delta SBE2}$ embryos. **(G–I)** Immunofluorescent staining for SF1 in E13.5 day VH parasagittal cryosections of control, $Shh^{\Delta SBE2/\Delta SBE2}$ and $Shh^{null/\Delta SBE2}$ embryos. Red arrows point to the region of the BH where SF1 expression is reduced or absent upon removal of SBE2 function. **(J–L)** Immunofluorescent staining for somatostatin in E13.5 day VH parasagittal cryosections of control, $Shh^{\Delta SBE2/\Delta SBE2}$ and $Shh^{null/\Delta SBE2}$ embryos. Red arrows point to the region of the BH where somatostatin is lost in $Shh^{null/\Delta SBE2}$ embryos. A zoomed in view of the region of somatostatin expression is presented in the green boxes in the upper right hand corner of **(J,K)**. AH- alar hypothalamus; BH- basal hypothalamus; IF- infundibulum; RP- Rathke's pouch. Scale bars are shown in the bottom right hand corner ($n = 3$).

SF1 was reduced (**Figure 7H**), while in $Shh^{null/\Delta SBE2}$ mutant embryos there was a complete loss of SF1 positive neurons (**Figure 7I**). Somatostatin (SOM) expressing neurons are a subset of GABAergic inhibitory neurons that are detected in varied nuclei of the hypothalamus, including the VMH and the arcuate nucleus, which serve to regulate cell proliferation ultimately affecting growth (Urban-Ciecko and Barth, 2016). In control embryos, SOM neurons were detected in the basal hypothalamic region corresponding to the arcuate nucleus at E13.5 (**Figure 7J**). No differences were detected in $Shh^{\Delta SBE2/\Delta SBE2}$ mutant embryos where comparable staining was detected (**Figure 7K**); however, in $Shh^{null/\Delta SBE2}$ mutant embryos no positive staining for SOM was detected in the VH (**Figure 7L**). These results indicate that low levels of *Shh* in the VH are sufficient to retain specification of SOM neurons, but higher levels of *Shh* activity are required to sustain and/or specify the SF1 neuronal population in the basal hypothalamus. In the $Shh^{null/\Delta SBE2}$ mutant embryos both of these populations were absent which indicates that early *Shh* activity is essential for the adequate establishment of both the SF1 and SOM neuronal populations of the basal hypothalamus.

Corman et al. (2018), have previously demonstrated that loss of *Shh* signalling directed by SBE2 leads to a loss or reduction of neuronal markers. Our data expand on these findings by demonstrating a previously unknown concentration dependent requirement for *Shh* in VH neuronal development whereby some neuronal populations, such SOM, are only affected when the levels of *Shh* are vastly reduced, as in $Shh^{null/\Delta SBE2}$ mutants. In contrast, the NKX2-1 and SF1 populations are affected by moderate reductions in the levels of *Shh* and further affected by greater loss of *Shh* signalling.

# DISCUSSION

## Secondary Enhancer Activity Contributes to *Shh* Expression After SBE2 Inactivation

Loss of SBE2 in $Shh^{\Delta SBE2/\Delta SBE2}$ homozygous mice did not cause lethality or overt phenotypic effects in the brain and craniofacial regions due to additional enhancer activity most likely from the broadly acting element SBE7. A multistep series of events generate the normal *Shh* expression levels in the ventral diencephalon of which SBE2 activity plays a later role. SBE7 is responsible for early *Shh* expression throughout the prechordal plate a tissue that underlies the developing brain, from as early as E7.5 (Sagai et al., 2019). SBE7, subsequently, drives *Shh* expression at low levels in the ventral midline of the developing forebrain throughout later developmental stages. By E9.5 SBE2 activation, which is dependent on the earlier SBE7 activity (Sagai et al., 2019), contributes to a substantially increased level of expression specifically in the ventral diencephalon.

SBE2 activity does not appear to be obligatory since in its absence the animals are viable and fertile; raising questions about the value of this enhancer to the embryo. In contrast, the deep conservation of this element strongly argues that SBE2 provides fitness to individuals and is crucial across the

vertebrate classes. Consequently, we argue that this is not an example of enhancer redundancy that commonly occurs in the mammalian genome (Osterwalder et al., 2018). Our analysis shows that expression of DV patterning genes is sensitive to a level of SHH which is perturbed in the absence of SBE2. SBE2 and SBE7 are components of a systematic temporal response required to reach sufficient SHH levels to attain the precise pattern of gene expression. Since further reduction of *Shh* levels (as in the $Shh^{null/\Delta SBE2}$ mutant) causes greater disruption to the expression of hypothalamic marker genes and perinatal lethality, it is reasonable to argue that, in the absence of SBE2, these animals are not fit in the wild. Disruption of neuronal populations seen in $Shh^{\Delta SBE2/\Delta SBE2}$ homozygous embryos, such as the reduction in the NKX2-1 and SF1 positive population, may lead to phenotypic effects on physiology, such as reproduction and energy balance. Indeed, specific depletion of the SF1 neuronal population of the VMH is known to be viable, however, the metabolic response of skeletal muscle is attenuated, revealing an effect upon metabolism (Fujikawa et al., 2016).

## SBE2 Mediated Expression Links Brain and Craniofacial Development

Heterozygous inactivating mutations in the *SHH* gene in patients cause HPE (Chiang et al., 1996; Ming and Muenke, 2002) while in mice complete loss of *Shh* leads to multiple phenotypic consequences including the absence of brain and craniofacial structures (Chiang et al., 1996). While these observations highlight the links between brain and craniofacial development, the question as to whether *Shh* signalling from the neuroectoderm is directly required for the development of the craniofacial elements has remained largely unanswered. Physical interactions between the brain and face begin early at the initial stages of facial formation (Marcucio et al., 2011). There are two fundamentally different mechanisms by which development of the face and brain may be interrelated; firstly, the developing brain serves as a dynamic architectural foundation upon which the face responds and develops and secondly, signalling directly from the brain to the cranium and face regulates morphogenesis.

In fish, *Shh* signalling from both the oral ectoderm and neural tissue is required for adequate progression of craniofacial development (Wada et al., 2005). In mammalian development, *Shh* signalling from the oral ectoderm, which underlies the cranial base and also neighbours the facial skeletal elements, has been demonstrated to be key in adequate craniofacial development. Depletion of signalling from the oral ectoderm leads to defects in the maxillary and mandibular bones, the palatine bones and the basisphenoid bone among others (Jeong et al., 2004). The present study addressed the role of SBE2 forebrain expression activity on the development of adjacent tissue which would be predicted to form the midline of the cranial floor. Loss of SBE2 in the presence of the *Shh* null allele leads to both lethality and craniofacial malformations. Defects were observed in multiple skeletal elements of the cranial base including the vomer bone and the basisphenoid bone, which resides below the pituitary glands and the hypothalamic tissue, demonstrating that *Shh*

signalling from the rostral diencephalon is directly required for adequate craniofacial development.

## SBE2 Affects Both AP and DV Patterning in the Hypothalamus

In addition to the craniofacial defects observed in the SBE2 mutant mouse lines, defects in hypothalamic development were also observed. This is perhaps unsurprising given that the region of *Shh* expression directed by SBE2 is the rostral diencephalon, one of the tissues from which the hypothalamus originates. However, the mode in which *Shh* regulates hypothalamic patterning and establishment appears to differ depending on the axis considered.

The AP axis was less sensitive to *Shh* levels of expression, whereby low, residual levels of signalling activity in the $Shh^{\Delta SBE2/\Delta SBE2}$ mutants were sufficient to sustain normal patterning. In contrast, further reduction of *Shh* expression in the $Shh^{null/\Delta SBE2}$ mutant embryos caused a loss of the anterior hypothalamic identity, which is promoted by *Shh*, in favour of the posterior hypothalamic identity. A shift in the anterior marker TCF4 was observed in the $Shh^{null/\Delta SBE2}$ mutant embryos, which contrasts previous observations (Zhao et al., 2012), where a shift in all other AP hypothalamic markers with the exception of TCF4 was found. In contrast, the lack of changes observed in pituitary marker expression agree with observations by Zhao et al. (2012) in SBE2-Cre $\Delta Shh$ mice, where pituitary markers were unperturbed, despite hypophyseal misplacement. Furthermore, SBE2-Cre $\Delta Shh$ mice displayed multiple invagination sites for RP, however only one site was seen in $Shh^{null/\Delta SBE2}$ embryos. The differences observed between our results and those of Zhao et al. (2012), likely reside in the different mouse lines used. Specifically, the use of SBE2-Cre to conditionally knock-down *Shh* activity may lead, firstly, to a temporal delay in the removal of *Shh* activity and, secondly, to a broader removal of *Shh* activity than that caused by direct deletion of SBE2. Notably, we also found that *Shh* is required for adequate development of hypothalamic neuronal populations which connect to the hypophyseal lobes and in turn, regulate hormonal release. These results demonstrate a dual role for *Shh* in ensuring hypophyseal function, directly in hypophyseal development and secondarily in regulating innervation.

In contrast to AP patterning, the DV hypothalamic axis was affected by *Shh* activity in a concentration dependent manner. This is apparent in the $Shh^{\Delta SBE2/\Delta SBE2}$ mutant embryos where defects in DV patterning, and also subsequent neuronal induction, were observed. These defects were far less severe than those observed in the $Shh^{null/\Delta SBE2}$ mutant embryos, where the disruption to DV development resulted in a complete loss of hypothalamic neuronal populations. The results presented regarding DV hypothalamic patterning are comparable to those described by Corman et al. (2018) where the same key neural tube patterning genes and subsequent neuronal regulators are involved. However, we have demonstrated a novel concentration dependent patterning activity of *Shh* in the hypothalamus, which has previously only been described in the neural tube. Moreover, the results demonstrate loss of neuronal populations beyond those of the dorsomedial, ventromedial and arcuate nuclei, additionally implicating neurons of the paraventricular

nucleus, which play a key role in hypophyseal regulation. Corman et al. (2018) also propose that NKX2-2 is expressed in a domain between dorsal PAX6 and ventral NKX2-1; however, our data suggest that NKX2-1 is expressed broadly across the entire ventral hypothalamic region, with NKX2-2 expressed in a subdomain of the ventral hypothalamus, in regions overlapping with NKX2-1. It is possible that the ventral hypothalamic markers induced by *Shh*, including NKX2-2 are responsible for inducing expression of NKX2-1, whereby ventral hypothalamic markers that are not completely absent in the $Shh^{null/\Delta SBE2}$ mutant embryos, sustain remaining NKX2-1 expression.

Similar to the patterning process in the neural tube, the response of different DV patterning transcription factors to *Shh* was concentration dependent. For example, NKX6-1 was ventrally displaced in the $Shh^{\Delta SBE2/\Delta SBE2}$ mutants, much like OLIG2. However, it was lost altogether in $Shh^{null/\Delta SBE2}$ mutant embryos, unlike OLIG2 which was further displaced; indicating that NKX6-1 is more sensitive to loss of *Shh* signalling than OLIG2. Similarly, in the neural tube OLIG2 responds to a wider range of *Shh* signalling levels than NKX6-1. This same variable sensitivity to *Shh* signalling was seen for the neuronal populations, whereby only some of the neuronal population that were disrupted in the $Shh^{null/\Delta SBE2}$ mutant embryos were also affected in the $Shh^{\Delta SBE2/\Delta SBE2}$ mutants; for example, NKX2-1 expression required higher levels of *Shh* expression than those needed for somatostatin. Moreover, *Shh* was found to only be essential to maintain some neuronal populations, like SF1 and somatostatin populations, which were completely absent in $Shh^{null/\Delta SBE2}$ mutants, whereas other populations such as ISL1 persist despite near complete loss of VH *Shh* signalling. Thus, early SBE2 directed *Shh* signalling directs subsequent DV patterning in a concentration dependent manner acting as a morphogen within ventral hypothalamic development, in which transcription factor expression patterns are controlled by *Shh* levels which in turn instruct ventral hypothalamic neuronal populations.

## SBE2 Coordinates Craniofacial Development and Patterning of the Hypothalamus

SBE2 regulates the expression of *Shh* in a region of the diencephalon in which SHH signalling coordinates development of both the diencephalon and the neighbouring tissue which forms the cranial and facial bones, skeletal elements which are in turn responsible for protecting the neural structures from external exposure. Homologues of the craniofacial bones disrupted in mouse are found in species of all vertebrate classes from fish to mammals (Maddin et al., 2016). In addition, the hypothalamus is an ancient brain centre critical for the production and release of key hormones (Xie and Dorsky, 2017). We suggest that deep in vertebrate evolution SBE2 activity arose as a means to govern VH development and as a consequence of hypothalamus proximity to craniofacial mesenchyme enabled *Shh* signalling to control formation of the bones to ensure its own protection. We have demonstrated that disruptions to coordinated development of the VH and

cranial vault in mice leads to phenotypic defects which reflect those seen for HPE patients. These results reveal not only that the interactions between the brain and the face display deeply conserved evolutionary roots, but also show the key importance of mouse models for addressing human disease phenotypes.

## DATA AVAILABILITY STATEMENT

The raw data produced for this study has been deposited in the Gene Expression Omnibus, Accession number GSE158074.

## ETHICS STATEMENT

All animal experiments were reviewed and approved by the University of Edinburgh Animal Welfare and Ethics Committee and were conducted with appropriate licensing under Animals (Scientific Procedures) Act 1986.

## AUTHOR CONTRIBUTIONS

RH: conceptualization. LL, NK, and ZC-S: methodology. ZC-S and DK: validation. ZC-S, JS, KG, PD, LR, MD, JT, and LL: investigation. ZC-S and RH: writing—original draft. DK, JS, and LL: writing—review and editing. ZC-S, KG, JS, and LL: visualization. DK, JS, and RH: supervision. DK and RH: funding acquisition. All authors contributed to the article and approved the submitted version.

## FUNDING

## ACKNOWLEDGMENTS

## SUPPLEMENTARY MATERIAL

The Supplementary Material for this article can be found online at: https://www.frontiersin.org/articles/10.3389/fcell.2021.595744/full#supplementary-material

## REFERENCES

Anderson, E., Devenney, P. S., Hill, R. E., and Lettice, L. A. (2014). Mapping the Shh long-range regulatory domain. *Development* 141, 3934–3943. doi: 10.1242/dev.108480

Balaskas, N., Ribeiro, A., Panovska, J., Dessaud, E., Sasai, N., Page, K. M., et al. (2012). Gene regulatory logic for reading the Sonic Hedgehog signaling gradient in the vertebrate neural tube. *Cell* 148, 273–284. doi: 10.1016/j.cell.2011.10.047

Blaess, S., Szabó, N., Haddad-Tóvolli, R., Zhou, X., and Álvarez-Bolado, G. (2014). Sonic hedgehog signaling in the development of the mouse hypothalamus. *Front. Neuroanat.* 8:156. doi: 10.3389/fnana.2014.00156

Buenrostro, J. D., Wu, B., Chang, H. Y., and Greenleaf, W. J. (2015). ATAC-seq: a method for assaying chromatin accessibility genome-wide. *Curr. Protoc. Mol. Biol.* 109, 21.29.1–21.29.9. doi: 10.1002/0471142727.mb2129s109

Burbridge, S., Stewart, I., and Placzek, M. (2016). Development of the neuroendocrine hypothalamus. *Compr. Physiol.* 6, 623–643. doi: 10.1002/cphy.c150023

Casillas, C., and Roelink, H. (2018). Gain-of-function Shh mutants activate Smo cell-autonomously independent of Ptch1/2 function. *Mech. Dev.* 153, 30–41. doi: 10.1016/j.mod.2018.08.009

Castinetti, F., Brinkmeier, M. L., Mortensen, A. H., Vella, K. R., Gergics, P., Brue, T., et al. (2015). ISL1 is necessary for maximal thyrotrope response to hypothyroidism. *Mol. Endocrinol.* 29, 1510–1521. doi: 10.1210/me.2015-1192

Chiang, C., Ying, L. T. T., Lee, E., Young, K. E., Corden, J. L., Westphal, H., et al. (1996). Cyclopia and defective axial patterning in mice lacking Sonic hedgehog gene function. *Nature* 383, 407–413. doi: 10.1038/383407a0

Choi, Y.-H., Fujikawa, T., Lee, J., Reuter, A., and Kim, K. W. (2013). Revisiting the ventral medial nucleus of the hypothalamus: the roles of SF-1 neurons in energy homeostasis. *Front. Neurosci.* 7:71. doi: 10.3389/fnins.2013.00071

Cong, L., Ran, F. A., Cox, D., Lin, S., Barretto, R., Habib, N., et al. (2013). Multiplex genome engineering using CRISPR/Cas systems. *Science (New York, N.Y.)* 339, 819–823. doi: 10.1126/science.1231143

Corman, T. S., Bergendahl, S. E., and Epstein, D. J. (2018). Distinct temporal requirements for Sonic hedgehog signaling in development of the tuberal hypothalamus. *Development (Cambridge, England)* 145:dev167379. doi: 10.1242/dev.167379

Croizier, S., Chometton, S., Fellmann, D., and Risold, P.-Y. (2015). Characterization of a mammalian prosencephalic functional plan. *Front. Neuroanat.* 8:161. doi: 10.3389/fnana.2014.00161

Dessaud, E., McMahon, A. P., and Briscoe, J. (2008). Pattern formation in the vertebrate neural tube: a sonic hedgehog morphogen-regulated transcriptional network. *Development* 135, 2489–2503. doi: 10.1242/dev.009324

Dessaud, E., Ribes, V., Balaskas, N., Yang, L. L., Pierani, A., Kicheva, A., et al. (2010). Dynamic assignment and maintenance of positional identity in the ventral neural tube by the morphogen sonic hedgehog. *PLoS Biol.* 8:e1000382. doi: 10.1371/journal.pbio.1000382

Dessaud, E., Yang, L. L., Hill, K., Cox, B., Ulloa, F., Ribeiro, A., et al. (2007). Interpretation of the sonic hedgehog morphogen gradient by a temporal adaptation mechanism. *Nature* 450, 717–720. doi: 10.1038/nature06347

Dworkin, S., Boglev, Y., Owens, H., Goldie, S., Dworkin, S., Boglev, Y., et al. (2016). The role of sonic hedgehog in craniofacial patterning, morphogenesis and cranial neural crest survival. *J. Dev. Biol.* 4:24. doi: 10.3390/jdb4030024

Ericson, J., Norlin, S., Jessell, T. M., and Edlund, T. (1998). Integrated FGF and BMP signaling controls the progression of progenitor cell differentiation and the emergence of pattern in the embryonic anterior pituitary. *Development (Cambridge, England)* 125, 1005–1015.

Ferrand, R. (1972). [Experimental study of the factors in cytological differentiation of the adenohypophysis in the chick embryo]. *Arch. Biol.* 83, 297–371.

Fujikawa, T., Castorena, C. M., Pearson, M., Kusminski, C. M., Ahmed, N., Battiprolu, P. K., et al. (2016). SF-1 expression in the hypothalamus is required for beneficial metabolic effects of exercise. *ELife* 5:e18206. doi: 10.7554/eLife.18206

Guillemot, F. (2007). Spatial and temporal specification of neural fates by transcription factor codes. *Development (Cambridge, England)* 134, 3771–3780. doi: 10.1242/dev.006379

Harfe, B. D., Scherz, P. J., Nissim, S., Tian, H., McMahon, A. P., and Tabin, C. J. (2004). Evidence for an expansion-based temporal shh gradient in specifying vertebrate digit identities. *Cell* 118, 517–528. doi: 10.1016/j.cell.2004.07.024

Hecksher-Sørensen, J., Hill, R. E., and Lettice, L. (1998). Double labeling for whole-mount in situ hybridization in mouse. *BioTechniques* 24, 914–918. doi: 10.2144/98246bm02

Hissnauer, T. N., Baranowsky, A., Pestka, J. M., Streichert, T., Wiegandt, K., Goepfert, C., et al. (2010). Identification of molecular markers for articular cartilage. *Osteoarthr. Cartil.* 18, 1630–1638. doi: 10.1016/J.JOCA.2010.10.002

Jeong, J. H., Mao, J. H., Tenzen, T., Kottmann, A. H., and McMahon, A. P. (2004). Hedgehog signaling in the neural crest cells regulates the patterning and growth of facial primordia. *Genes Dev.* 18, 937–951. doi: 10.1101/gad.1190304

Jeong, Y., El-Jaick, K., Roessler, E., Muenke, M., and Epstein, D. J. (2006). A functional screen for sonic hedgehog regulatory elements across a 1 Mb interval identifies long-range ventral forebrain enhancers. *Development* 133, 761–772. doi: 10.1242/dev.02239

Jeong, Y., Leskow, F. C., El-Jaick, K., Roessler, E., Muenke, M., Yocum, A., et al. (2008). Regulation of a remote Shh forebrain enhancer by the Six3 homeoprotein. *Nat. Genet.* 40, 1348–1353. doi: 10.1038/ng.230

Kawamura, K., and Kikuyama, S. (1995). Induction from posterior hypothalamus is essential for the development of the pituitary proopiomelacortin (POMC) cells of the toad (Bufo japonicus). *Cell Tissue Res.* 279, 233–239. doi: 10.1007/bf00318479

Kim, N., Park, C., Jeong, Y., and Song, M.-R. (2015). Functional diversification of motor neuron-specific *Isl1* enhancers during evolution. *PLoS Genet.* 11:e1005560. doi: 10.1371/journal.pgen.1005560

Larsson, A. J. M., Johnsson, P., Hagemann-Jensen, M., Hartmanis, L., Faridani, O. R., Reinius, B., et al. (2019). Genomic encoding of transcriptional burst kinetics. *Nature* 565, 251–254. doi: 10.1038/s41586-018-0836-1

Letelier, J., De La Calle-Mustienes, E., Pieretti, J., Naranjo, S., Maeso, I., Nakamura, T., et al. (2018). A conserved Shh cis-regulatory module highlights a common developmental origin of unpaired and paired fins. *Nat. Genet.* 50, 504–509. doi: 10.1038/s41588-018-0080-5

Lettice, L. A., Williamson, I., Devenney, P. S., Kilanowski, F., Dorin, J., and Hill, R. E. (2014). Development of five digits is controlled by a bipartite long-range cis-regulator. *Development* 141, 1715–1725. doi: 10.1242/dev.095430

Lu, F., Kar, D., Gruenig, N., Zhang, Z. W., Cousins, N., Rodgers, H. M., et al. (2013). Rax is a selector gene for mediobasal hypothalamic cell types. *J. Neurosci.* 33, 259–272. doi: 10.1523/JNEUROSCI.0913-12.2013

Mackenzie, M. A. F., Jordan, S. A., Budd, P. S., and Jackson, I. J. (1997). Activation of the receptor tyrosine kinase kit is required for the proliferation of melanoblasts in the mouse embryo. *Dev. Biol.* 192, 99–107. doi: 10.1006/DBIO.1997.8738

Maddin, H. C., Piekarski, N., Sefton, E. M., and Hanken, J. (2016). Homology of the cranial vault in birds: new insights based on embryonic fate-mapping and character analysis. *R. Soc. Open Sci.* 3:160356. doi: 10.1098/rsos.160356

Marcorelles, P., and Laquerriere, A. (2010). Neuropathology of holoprosencephaly. *Am. J. Med. Genet. Part C Semin. Med. Genet.* 154C, 109–119. doi: 10.1002/ajmg.c.30249

Marcucio, R. S., Young, N. M., Hu, D., and Hallgrimsson, B. (2011). Mechanisms that underlie co-variation of the brain and face. *Genesis* 49, 177–189. doi: 10.1002/dvg.20710

Ming, J. E., and Muenke, M. (2002). Multiple hits during early embryonic development: digenic diseases and holoprosencephaly. *Am. J. Hum. Genet.* 71, 1017–1032. doi: 10.1086/344402

Nagy, A., Gertsenstein, M., Vintersten, K., and Behringer, R. (2009a). Alizarin red staining of post-natal bone in mouse. *Cold Spring Harb. Protoc.* 2009:db.rot5171. doi: 10.1101/pdb.prot5171

Nagy, A., Gertsenstein, M., Vintersten, K., and Behringer, R. (2009b). Alcian blue staining of the mouse fetal cartilaginous skeleton. *Cold Spring Harb. Protoc.* 2009:db.rot5169. doi: 10.1101/pdb.prot5169

Nord, A. S., Blow, M. J., Attanasio, C., Akiyama, J. A., Holt, A., Hosseini, R., et al. (2013). Rapid and pervasive changes in genome-wide enhancer usage during mammalian development. *Cell* 155, 1521–1531. doi: 10.1016/j.cell.2013.11.033

Ohyama, K., Ellis, P., Kimura, S., and Placzek, M. (2005). Directed differentiation of neural cells to hypothalamic dopaminergic neurons. *Development (Cambridge, England)* 132, 5185–5197. doi: 10.1242/dev.02094

Osterwalder, M., Barozzi, I., Tissiéres, V., Fukuda-Yuzawa, Y., Mannion, B. J., Afzal, S. Y., et al. (2018). Enhancer redundancy provides phenotypic robustness in mammalian development. *Nature* 554, 239–243. doi: 10.1038/nature25461

Pai, Y. J., Leung, K. Y., Savery, D., Hutchin, T., Prunty, H., Heales, S., et al. (2015). Glycine decarboxylase deficiency causes neural tube defects and features of non-ketotic hyperglycinemia in mice. *Nat. Commun.* 6:6388. doi: 10.1038/ncomms7388

Pontecorvi, M., Goding, C. R., Richardson, W. D., and Kessaris, N. (2008). Expression of Tbx2 and Tbx3 in the developing hypothalamic–pituitary axis. *Gene Expr. Patterns* 8, 411–417. doi: 10.1016/j.gep.2008.04.006

Sagai, T., Amano, T., Maeno, A., Ajima, R., and Shiroishi, T. (2019). SHH signaling mediated by a prechordal and brain enhancer controls forebrain organization. *Proc. Natl. Acad. Sci. U.S.A.* 116, 23636–23642. doi: 10.1073/pnas.1901732116

Sander, M., Paydar, S., Ericson, J., Briscoe, J., Berber, E., German, M., et al. (2000). Ventral neural patterning by Nkx homeobox genes: Nkx6.1 controls somatic motor neuron and ventral interneuron fates. *Genes Dev.* 14, 2134–2139. doi: 10.1101/gad.820400

Schwind, J. L. (1928). The development of the hypophysis cerebri of the albino rat. *Am. J. Anat.* 41, 295–319. doi: 10.1002/aja.1000410206

Sharpe, J. (2003). Optical projection tomography as a new tool for studying embryo anatomy. *J. Anat.* 202, 175–181. doi: 10.1046/J.1469-7580.2003.00155.X

Takuma, N., Sheng, H. Z., Furuta, Y., Ward, J. M., Sharma, K., Hogan, B. L., et al. (1998). Formation of Rathke's pouch requires dual induction from the diencephalon. *Development (Cambridge, England)* 125, 4835–4840.

Treier, M., Gleiberman, A. S., O'Connell, S. M., Szeto, D. P., McMahon, J. A., McMahon, A. P., et al. (1998). Multistep signaling requirements for pituitary organogenesis in vivo. *Genes Dev.* 12, 1691–1704. doi: 10.1101/gad.12.11.1691

Tsukiji, N., Amano, T., and Shiroishi, T. (2014). A novel regulatory element for Shh expression in the lung and gut of mouse embryos. *Mech. Dev.* 131, 127–136. doi: 10.1016/J.MOD.2013.09.003

Urban-Ciecko, J., and Barth, A. L. (2016). Somatostatin-expressing neurons in cortical networks. *Nat. Rev. Neurosci.* 17, 401–409. doi: 10.1038/nrn.2016.53

Wada, N., Javidan, Y., Nelson, S., Carney, T. J., Kelsh, R. N., and Schilling, T. F. (2005). Hedgehog signaling is required for cranial neural crest morphogenesis and chondrogenesis at the midline in the zebrafish skull. *Development (Cambridge, England)* 132, 3977–3988. doi: 10.1242/dev.01943

Williamson, I., Kane, L., Devenney, P. S., Flyamer, I. M., Anderson, E., Kilanowski, F., et al. (2019). Developmentally regulated Shh expression is robust to TAD perturbations. *Development (Cambridge)* 146:dev179523. doi: 10.1242/dev.179523

Xie, Y., and Dorsky, R. I. (2017). Development of the hypothalamus: conservation, modification and innovation. *Development (Cambridge, England)* 144, 1588–1599. doi: 10.1242/dev.139055

Yee, S. P., and Rigby, P. W. J. (1993). The regulation of myogenin gene expression during the embryonic development of the mouse. *Genes Dev.* 7, 1277–1289. doi: 10.1101/gad.7.7a.1277

Zhao, L., Zevallos, S. E., Rizzoti, K., Jeong, Y., Lovell-Badge, R., and Epstein, D. J. (2012). Disruption of SoxB1-dependent sonic hedgehog expression in the hypothalamus causes septo-optic dysplasia. *Dev. Cell* 22, 585–596. doi: 10.1016/J.DEVCEL.2011.12.023